Atmosphere surface storm track response to resolved ocean mesoscale in two sets of global climate model experiments

R. Justin Small, Rym Msadek, Young-Oh Kwon, James F. Booth & Colin Zarzycki

Climate Dynamics
Observational, Theoretical and Computational Research on the Climate System

ISSN 0930-7575

Clim Dyn
DOI 10.1007/s00382-018-4237-9

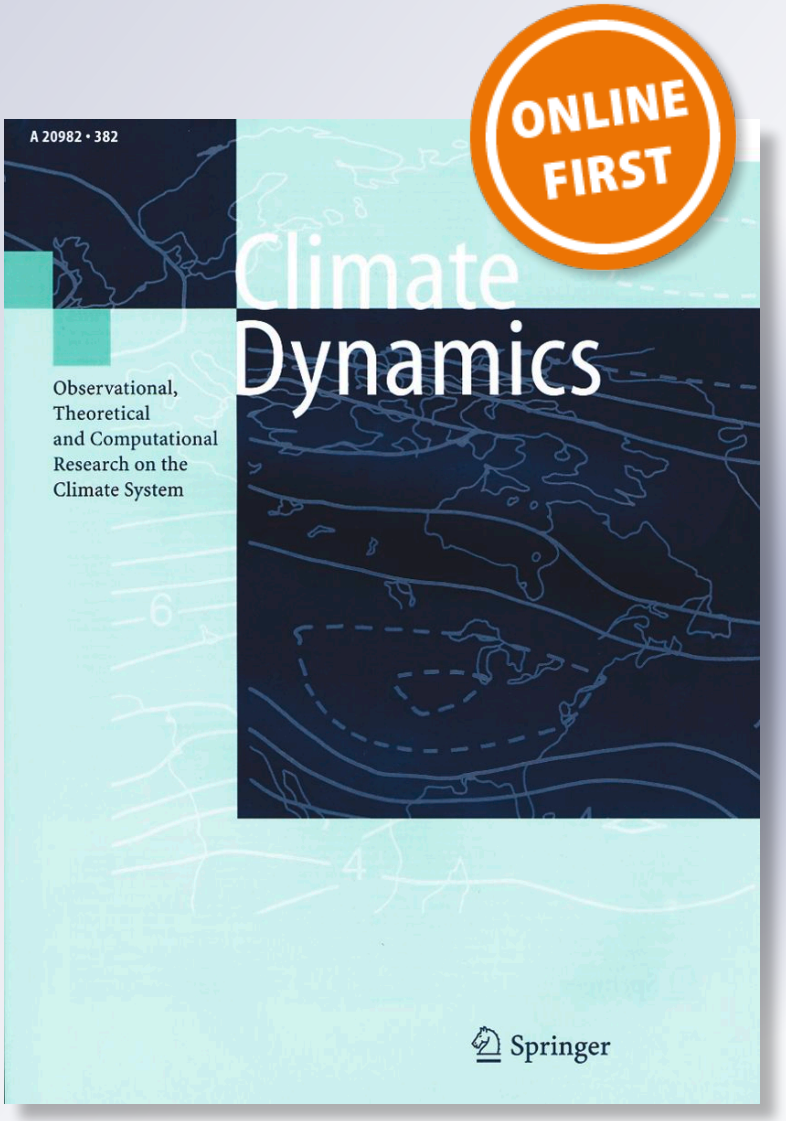

Springer

Climate Dynamics
https://doi.org/10.1007/s00382-018-4237-9

Atmosphere surface storm track response to resolved ocean mesoscale in two sets of global climate model experiments

R. Justin Small[1] · Rym Msadek[2] · Young-Oh Kwon[3] · James F. Booth[4] · Colin Zarzycki[5]

Received: 31 October 2017 / Accepted: 3 May 2018

Abstract

It has been hypothesized that the ocean mesoscale (particularly ocean fronts) can affect the strength and location of the overlying extratropical atmospheric storm track. In this paper, we examine whether resolving ocean fronts in global climate models indeed leads to significant improvement in the simulated storm track, defined using low level meridional wind. Two main sets of experiments are used: (i) global climate model Community Earth System Model version 1 with non-eddy-resolving standard resolution or with ocean eddy-resolving resolution, and (ii) the same but with the GFDL Climate Model version 2. In case (i), it is found that higher ocean resolution leads to a reduction of a very warm sea surface temperature (SST) bias at the east coasts of the U.S. and Japan seen in standard resolution models. This in turn leads to a reduction of storm track strength near the coastlines, by up to 20%, and a better location of the storm track maxima, over the western boundary currents as observed. In case (ii), the change in absolute SST bias in these regions is less notable, and there are modest (10% or less) increases in surface storm track, and smaller changes in the free troposphere. In contrast, in the southern Indian Ocean, case (ii) shows most sensitivity to ocean resolution, and this coincides with a larger change in mean SST as ocean resolution is changed. Where the ocean resolution does make a difference, it consistently brings the storm track closer in appearance to that seen in ERA-Interim Reanalysis data. Overall, for the range of ocean model resolutions used here (1° versus 0.1°) we find that the differences in SST gradient have a small effect on the storm track strength whilst changes in absolute SST between experiments can have a larger effect. The latter affects the land–sea contrast, air–sea stability, surface latent heat flux, and the boundary layer baroclinicity in such a way as to reduce storm track activity adjacent to the western boundary in the N. Hemisphere storm tracks, but strengthens the storm track over the southern Indian Ocean. A note of caution is that the results are sensitive to the choice of storm track metric. The results are contrasted with those from a high resolution coupled simulation where the SST is smoothed for the purposes of computing air–sea fluxes, an alternative method of testing sensitivity to SST gradients.

1 Introduction

Extratropical storm tracks are a major component of the dynamical climate system, driving the extratropical atmospheric jets (Lorenz and Hartmann 2001) as well as affecting weather variability, surface waves, and sea level variability. There is some evidence that high resolution atmosphere models can change some aspects of the storm tracks such as the distribution of extremes, by better resolving atmospheric fronts and small mesoscale systems (Willison et al. 2013). In addition, high resolution ocean models produce sharp sea surface temperature (SST) gradients at ocean fronts, and these can influence the low level atmospheric baroclinicity (Nakamura et al. 2004, 2008) and the turbulent heat transfer across the air-sea interface (Taguchi et al. 2009). The ocean mesoscale features exhibit strong lateral surface temperature

Electronic supplementary material The online version of this article (https://doi.org/10.1007/s00382-018-4237-9) contains supplementary material, which is available to authorized users.

✉ R. Justin Small
jsmall@ucar.edu

[1] Climate and Global Dynamics Division, National Center for Atmospheric Research, 1850 Table Mesa Drive, Boulder, CO 80305, USA

[2] CECI UMR 5318, CNRS/CERFACS, Toulouse, France

[3] Woods Hole Oceanographic Institution, Woods Hole, USA

[4] City College, City University of New York, New York, USA

[5] Climate and Global Dynamics, National Center for Atmospheric Research, Boulder, CO 80305, USA

Published online: 11 May 2018

Table 1 List of experiments, model systems, component resolutions, and years analyzed

Experiment name	Model system	Ocean resolution	Atmosphere resolution	Years analyzed and notes
CESM-HR	CESM1	0.1°	0.25°	Years 60–90
CESM-LR	CESM1	1°	0.25°	Years 60–90
CESM-A	CESM1	0.25° daily analyzed SST	0.25°	2 cycles of 7 years each, 2003–2009. No-active ocean, Reynolds et al. (2007) SST
GFDL-CM-HR	GFDL-CM	0.1°	0.5°	Years 111–140
GFDL-CM-LR	GFDL-CM	1°	0.5°	Years 111–140
SmthSST	CESM1	0.1°	0.25°	10 year run only, initialized from year 60 of CESM-HR. SST smoothed for air-sea fluxes

contrasts that give rise to spatially varying turbulent heat fluxes at the ocean surface, and gradients in the overlying air temperature and moisture. Thus, it may be expected that high-resolution global climate models will produce different storm tracks than their standard resolution equivalents. This paper investigates whether this expectation is true, using coupled climate models run with a high atmosphere resolution coupled to two different ocean resolutions including some with specialized treatment of the SST.

A major question for this study is whether the storm track responds more closely to differences in SST gradient between simulations, or just to differences in SST. The former affects the low level baroclinicity in the atmosphere (Nakamura et al. 2004, 2008; Taguchi et al. 2009; Small et al. 2014a) whilst the latter affects the supply of latent heat to the storms (Kuo et al. 1991; Stoelinga et al. 1996; Businger et al. 2005) and also vertical mixing of momentum (Booth et al. 2010; Liu et al. 2013). In a series of regional atmosphere model sensitivity experiments for a single case in the NW Atlantic, Booth et al. (2012) found that changes in absolute SST had more influence on storm development than changes in the gradient of SST. In contrast, Sheldon et al. (2017) noted that both the thermodynamic effect (due to warm absolute SST) and the dynamic effect (due to SST gradient) were important to the extent of ascent over the Gulf Stream. This paper will address the role of absolute SST versus SST gradient for the long-term mean storm track.

This paper is novel in that it utilizes fully coupled models, which include interactive exchanges of fluxes and momentum between the ocean and the atmosphere and have hence additional complexities compared to the atmosphere-only simulations analyzed in most of the previous studies (including Woollings et al. 2010; Piazza et al. 2016), such as mean state SST biases, which we find to be of major importance in this paper. Further, we use state-of-the-art model components applied at some of the highest horizontal resolutions currently found in climate models.

The initial focus of this paper is on storm track defined in terms of meridional wind variance. The meridional wind is a traditional measure of the storm track, as discussed in Trenberth (1991, his schematic Fig. 1), and in Hoskins and Hodges (2002, their schematic Fig. 1), and is closely related to other climatically important quantities such as temperature variability, due to meridional advection across mean temperature gradients. Later in the paper other metrics are introduced for comparison.

The paper is structured as follows. Section 2 presents the models, experiments and metrics to be used. The global and regional sensitivity of the storm track to ocean resolution in global climate models is described in Sect. 3, where the storm track is defined in terms of synoptic variability of low level meridional winds. Section 4 analyzes various factors that potentially explain the changes in storm track with resolution. A comparison of different storm track metrics is given in Sect. 5, including precipitation metrics and Lagrangian storm tracking. Section 6 presents a discussion on the role of absolute SST versus SST gradient in affecting storm track, including results from a coupled sensitivity experiment, where the SST used to compute air-sea fluxes is spatially smoothed, as well as discussion on the differences between Eulerian and Lagrangian storm track metrics. Finally, conclusions are made in Sect. 7.

2 Experiments and methods

2.1 Climate model experiments

Model experiments to isolate the impact of ocean mesoscale and ocean resolution are performed within two modelling systems: the Community Earth System Model (CESM1) and the GFDL Climate Model (CM2). For reference, Table 1 lists all experiments.

2.1.1 CESM

CESM1 (Hurrell et al. 2013) as applied here is composed of the Community Atmosphere Model 5.2 using a spectral element dynamical core (Park et al. 2014), Parallel Ocean Program version 2 (POP2, Smith et al. 2010), Community Ice Code version 4 (Hunke and Lipscomb 2008), Community Land Model version 4 (Lawrence et al. 2011) and CESM Coupler 7 with the Large and Yeager (2009) air-sea flux routine. The highest resolution simulation used here, with 0.25° resolution in the atmosphere and nominal 0.1° in the ocean, is described in full in Small et al. (2014b). It was run for 100 years under "present-day" (year 2000) greenhouse gas conditions and is referred to here as CESM-High ocean Resolution (CESM-HR). This is compared to a simulation with the same 0.25° atmosphere resolution but a nominal 1° ocean resolution, where ocean eddies are parameterized (Gent and McWilliams 1990). This 90-year run under fixed year 2000 conditions is referred to as CESM-Low ocean Resolution (CESM-LR), and is different to the CESM with standard resolution described in Small et al. (2014b), which had atmosphere resolution of 1°. All experiments except SmthSST (described in Sect. 6.1) are of at least 90 years in length, and the analysis described in this paper uses 30-year segments from a latter part of the simulations (Table 1).

2.1.2 GFDL CM

The GFDL global coupled models (GFDL-CM) that are analyzed here are the GFDL Forecast-oriented Low Ocean Resolution (FLOR; Vecchi et al. 2014) and the GFDL CM2.6 (Delworth et al. 2012; Griffies et al. 2014). The two configurations share the same atmosphere and land components which have a horizontal resolution of approximately 50 km × 50 km using a cubed sphere finite volume dynamical core (Putman and Lin 2007). The ocean and sea ice components in FLOR are based on the low-resolution GFDL CM2.1 model (Delworth et al. 2006), with a nominal horizontal grid spacing of 1°. CM2.6 has the same atmosphere model as FLOR but uses a higher-resolution ocean with a nominally 0.1° grid spacing that resolves the Rossby radius in most regions equatorward of 50° (Delworth et al. 2012; Griffies et al. 2014). In the following, for consistency with our CESM nomenclature, FLOR will be referred to as GFDL-CM-LR and CM2.6 as GFDL-CM-HR. The models were run for several hundred years under fixed preindustrial (1860) greenhouse gas conditions and the diagnostics used in this paper are based on years 111–140 (see Table 1). The fact that CESM and GFDL CM were initialized for different years (year 2000 versus year 1860 respectively) is not expected to make a major impact on the results, as most of our comparisons in this paper are between a pair of simulations with the same model and start point. Further when comparing CESM and GFDL-CM we note that the local changes in SST due to model resolution are much larger than those expected from climate change between 1860 and 2000. However, changes to the background storm track due to climate change may still have some impact on these latter comparisons, and so we focus on effects that can be robustly attributable to changes in SST or SST gradient. (Differences between GFDL-CM and CESM can also be due to the different model physics, as discussed in Sect. 7).

2.2 Methods

In this paper, Eulerian storm track statistics are computed as the standard deviation of daily-differenced state variables. The daily difference method (Wallace et al. 1988; Guo et al. 2009; Booth et al. 2017) captures most elements of synoptic variability, and analysis using more traditional bandpass methods leads to similar conclusions. The output used for this approach are: daily averages of meridional wind, at 10 m and at 850 hPa, daily averaged precipitation, and latent heat flux. Note that the CESM 10 m storm track uses a neutral equivalent wind (Liu and Tang 1996). Very similar responses were obtained using the actual 10 m wind and the wind at the lowest model level (see Booth et al. 2017), where it is explained that influence of the surface stability on the difference between actual and neutral 10 m winds is weak in the strong wind regions of the storm track.

A Lagrangian feature-tracking approach is also used for CESM, following storms via their surface pressure centers using the TempestExtremes software package (Ullrich and Zarzycki 2017). The method follows a standard "detect-and-stitch" strategy used by many centers for tracking pointwise features (e.g., Neu et al. 2013). TempestExtremes was applied to 20 years of 6-hourly data from the CESM-LR and CESM-HR simulations on the native atmospheric grid, following local minima in the surface pressure field by a closed contour of at least 2 hPa within a 4° box. Storms must persist for 24 h to be retained. Track density was calculated and is defined as the number of 6-hourly points from all trajectories that fall in 6° × 6° boxes. The approach allows for discrete classification of individual tracks and therefore identification of statistics such as track density and mean intensity (e.g. Hoskins and Hodges 2002; Neu et al. 2013).

For the Eulerian approach, statistical significance is determined using the Student's *t* test. 95% significance of the difference of means is tested as in Small et al. (2014a), where each DJF season is considered a sample, and tests to remove the effect of serial autocorrelation are performed.

The baroclinicity used here is defined as the maximum Eady growth rate, and we compute the magnitude of the long-term time-mean baroclinicity vector, as given in Nakamura and Yamane (2009) and Small et al. (2014a, their Sect. 5.2).

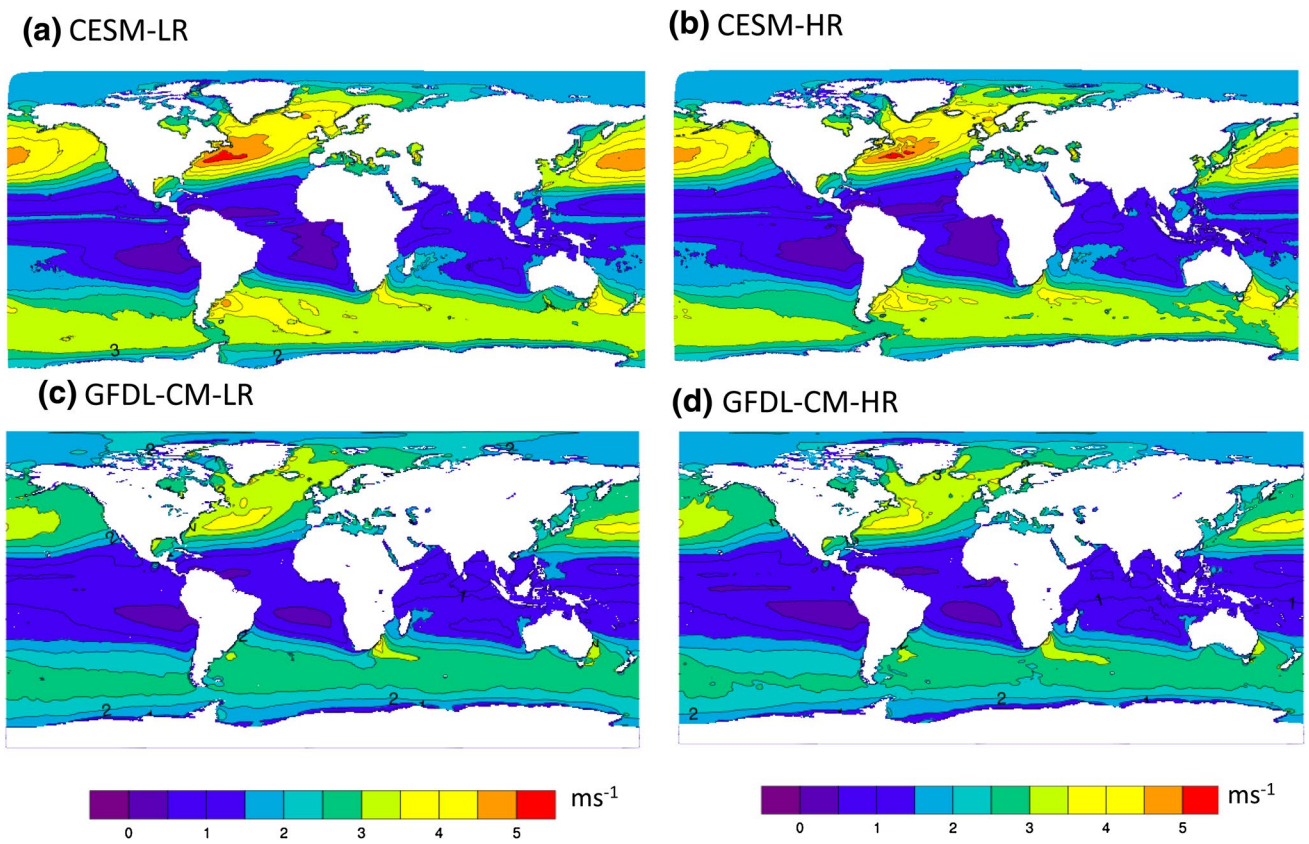

Fig. 1 The surface storm track in DJF, based on 10 m meridional wind, from **a, b** CESM and **c, d** GFDL-CM. Cases with standard resolution ocean are shown in **a, c** and with high resolution ocean in **b, d**. Color bar for all panels is shown at bottom

$$|\underline{\sigma}| = 0.31 \frac{g}{N\theta_0} \left| \left(-\frac{\partial \theta}{\partial y}, \frac{\partial \theta}{\partial x} \right) \right|$$

3 Synoptic variability in fully coupled experiments

3.1 Global view of storm track

The boreal winter (DJF) surface storm track in CESM and GFDL CM with low resolution ocean models shows the familiar maxima over the western North Atlantic and North Pacific Ocean basins, and a weaker, more circumglobal storm track in the Southern Hemisphere (Austral summer) (Fig. 1a, c). Moving to a high resolution ocean does not lead to a large scale increase in the magnitude of the surface storm track, in either model (Fig. 1b, d). The peak magnitudes of the North Atlantic and North Pacific storm tracks are very similar across resolution both in GFDL CM (Fig. 1c, d) and in CESM (Fig. 1a, b), and the southern hemisphere storm track shows some regions of reduction of strength in CESM with increasing resolution (e.g. directly west and east of South America, Fig. 1a,b), whilst there is a slight increase south and east of South Africa in GFDL CM with increasing resolution (Fig. 1c, d). Note that similar conclusions hold for the Southern Hemisphere in Austral winter, JJA (not shown).

In general, surface synoptic variability is stronger in CESM than in GFDL CM (and most other models and reanalyses). Booth et al. (2017), found that four of the CMIP5 models, including CESM, had unusually strong surface storm tracks compared to ERA-Interim (Dee et al. 2011) and the majority of CMIP5 models. However, the free troposphere storm track in these four models was comparable to the other models and reanalysis. The cause of this boundary layer overestimation of winds in CESM (and also of surface stress) is not currently known but is being investigated (Simpson et al. 2018).

The reasons for the apparent lack of overall strengthening of the storm tracks in response to the stronger SST gradients seen at high ocean resolution are discussed in detail in Sects. 4, 5, and 6.1. Before that, some regional characteristics of the simulations are discussed, together with supporting simulations in atmosphere-only mode and comparison with Reanalysis data.

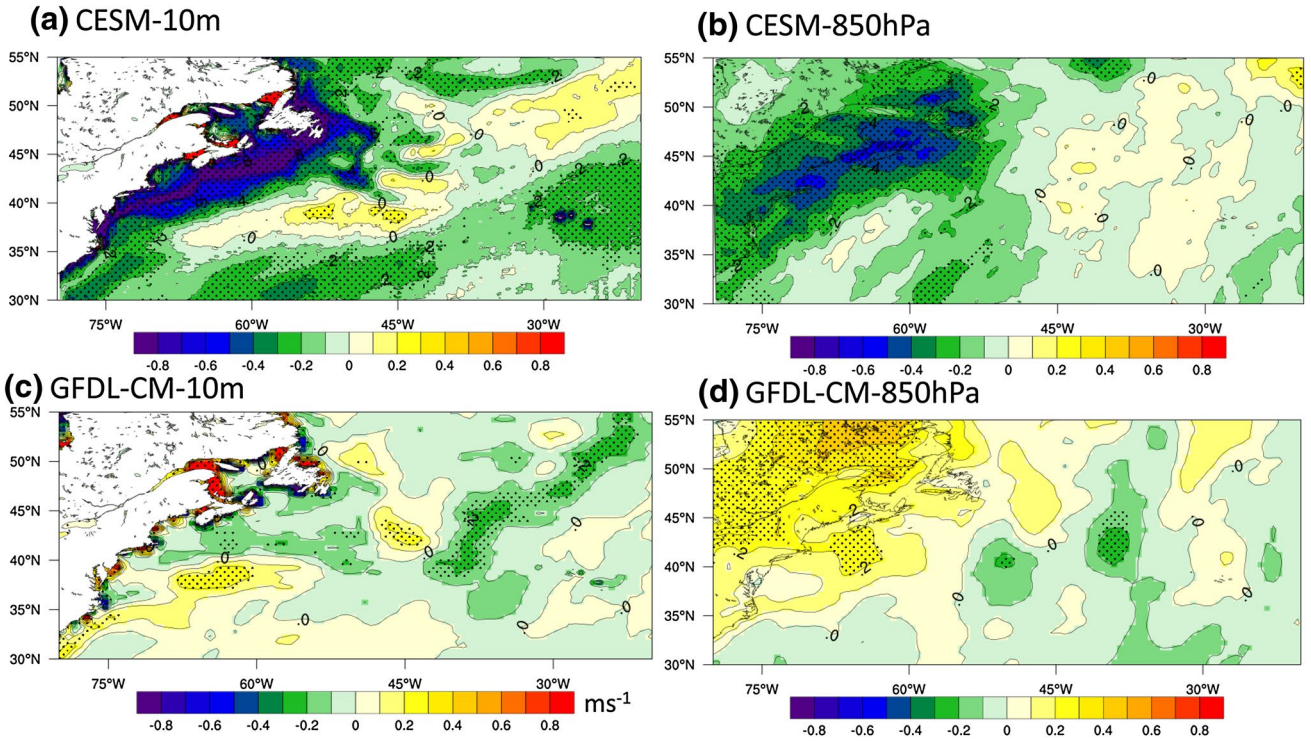

Fig. 2 North-west Atlantic storm track differences between high resolution and low resolution runs (HR minus LR). **a, c** for 10 m meridional wind, **b, d** for meridional wind at 850 hPa, all for DJF. Top panels: CESM, bottom panels: GFDL-CM. Statistically significant differences at 95% according to the *t* test are stippled, and in the left panels the land is masked out

3.2 Regional aspects of storm track

We discuss here three regional cases: firstly, in most detail, the Northwest Atlantic, followed by comparison with the Northwest Pacific and southern Indian Ocean.

3.2.1 Northwest Atlantic

The North Atlantic surface storm track in CESM-HR maximizes offshore (Fig. 1b), in the approximate location of the Gulf Stream extension, as seen in reanalysis and observations (Booth et al. 2010, 2017), whilst it extends more coastward in CESM-LR (Fig. 1a). As a consequence, the surface storm track in the CESM-HR is reduced by as much as 0.8 m/s, or about 20%, off the U.S. east coast compared to CESM-LR (Fig. 2a). Although there is a weak increase of the storm track further offshore, some of this is not significant (Fig. 2a). The reduction in storm track off the U.S. east coast is not just a near-surface change, as illustrated by the statistically significant 850-hPa storm track difference fields for CESM (Fig. 2b). However, the surface storm track decreases more than the 850 hPa storm track, so that the ratio of the surface to 850 hPa storm track is reduced at high resolution: indicative of a more stable environment induced by the reduction of SST off the U.S. east coast in the high-resolution case (see Fig. 9a below). This issue is further discussed in Booth et al. (2017) (see their Fig. 10). These results may be interpreted as the high resolution model pushing the peak storm track offshore, as the Gulf Stream position is more realistically simulated in the high resolution, instead of immediately off the coast, as found in shorter AMIP runs by Woollings et al. (2010). (In Sects. 3.3 and 3.4 the question of whether this makes the storm track more realistic is addressed.)

The GFDL CM resolution comparison does show some surface storm track weakening off the coast and strengthening near the Gulf Stream extension (Fig. 2c), but the amplitudes of the differences are much weaker than in CESM and the patterns are less coherent. In GFDL CM, the positive and negative differences are more comparable in amplitude than is seen in CESM where the negative pole is dominant. This is likely due to the more symmetric positive and negative differences between the high and low-resolution SST in GFDL CM as compared to CESM, as discussed in Sect. 4 (Fig. 9a, b). The storm track change due to increased resolution at 850 hPa shows a strengthening of the northwestern part of the storm track and a slight weakening of the southeastern part in GFDL CM, with a significant positive response over the Northeast American continent (Fig. 2d). This pattern is not obviously related to the weak SST difference shown

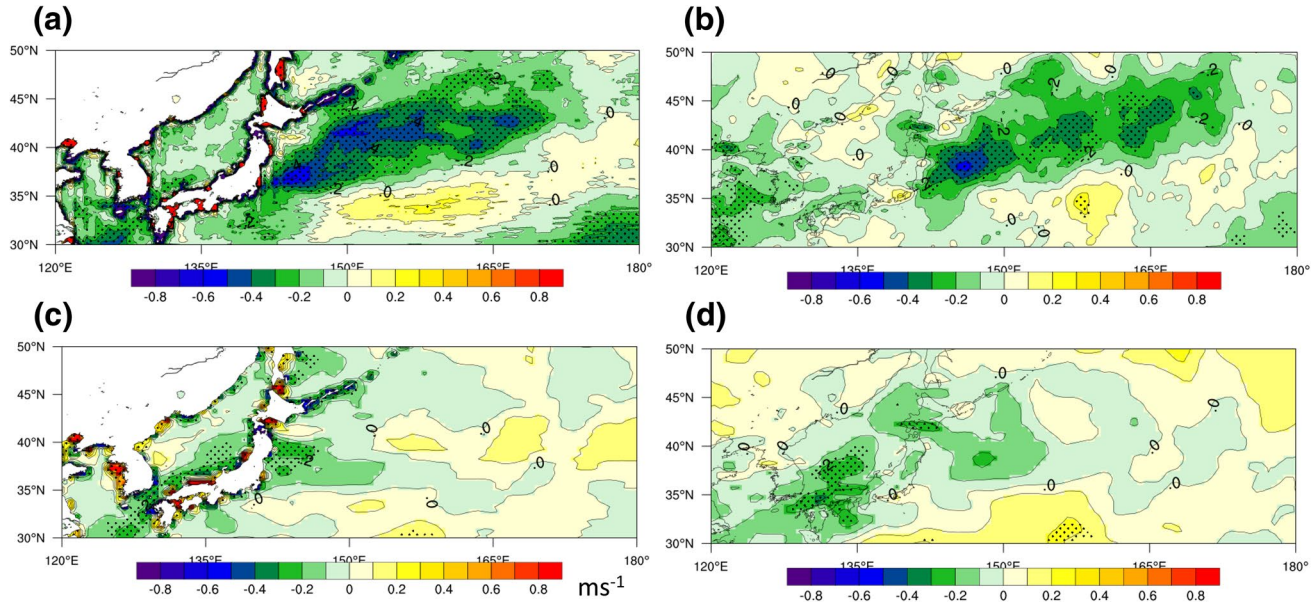

Fig. 3 As Fig. 2 but for the North-West Pacific in DJF

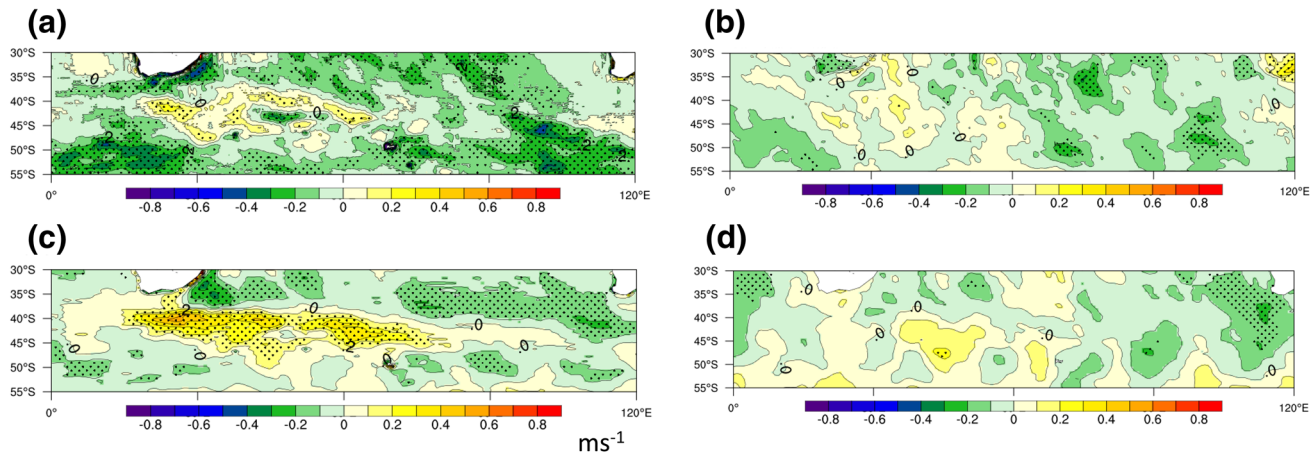

Fig. 4 As Fig. 2 but for the Southern Indian Ocean in DJF

in Fig. 9b below, however a weak increase in baroclinicity at 850 hPa was seen over the Continent in GFDL-CM-HR compared to GFDL-CM-LR (not shown).

3.2.2 Northwest Pacific

In CESM the storm track sensitivity to resolution is somewhat similar in the Northwest Pacific to that in the Northwest Atlantic, with a statistically significant local reduction of storm track east of Japan in CESM-HR, at 10 m and at 850 hPa (Fig. 3a, b). However, this reduction in storm track is less tied to the land-sea boundary than seen in the North Atlantic, and instead is located downstream. In GFDL CM, the pattern is similar, but with weaker amplitude than in CESM, and again not very significant (Fig. 3c, d).

3.2.3 Southern Indian Ocean

In the southern Indian Ocean in DJF, in CESM the change to the storm track at 10 m is modest, with local differences of less than 0.4 m/s (~ 10%, Fig. 4a) and at 850 hPa differences are mostly insignificant (Fig. 4b). In GFDL CM, the Indian Ocean 10 m storm track differences are more notable (visible in Fig. 1d, as an extended maximum, see also Fig. 4c), and stronger than in CESM, but with a similar spatial pattern to CESM. Again there is a lack of significant difference at 850 hPa (Fig. 4d). For reference, the storm track sensitivity

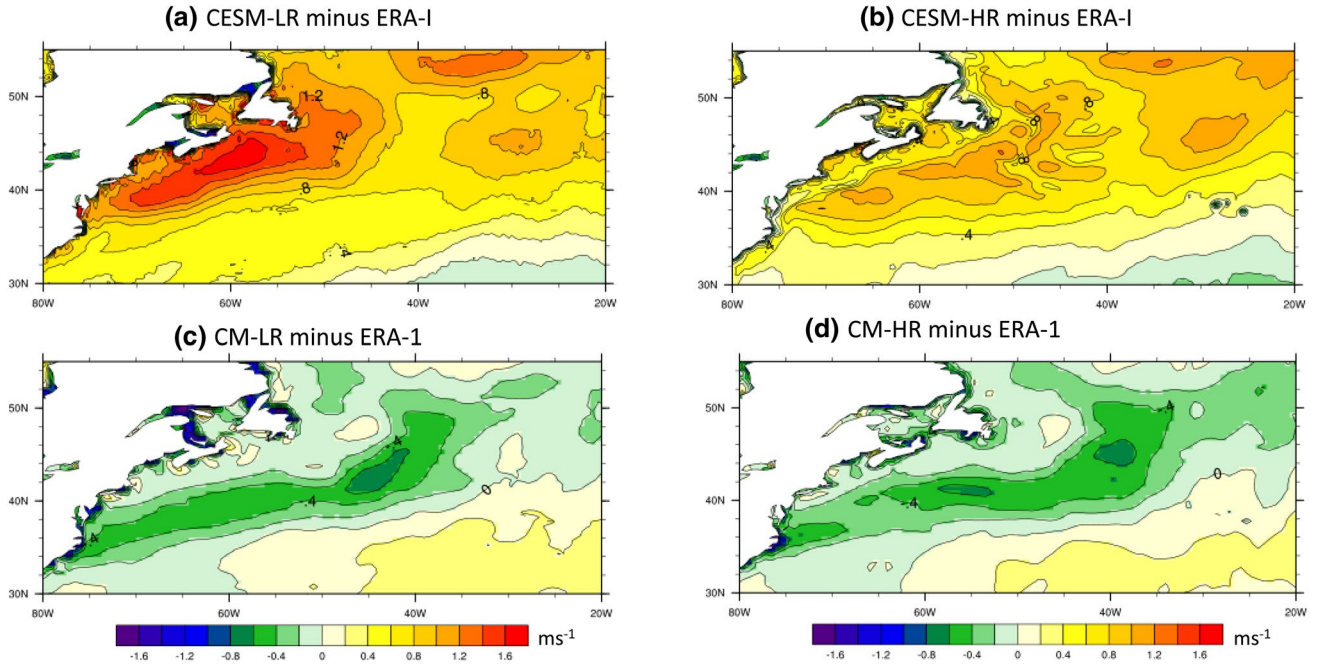

Fig. 5 Difference between surface storm track in climate models and that in ERA-Interim, for DJF in the North-West Atlantic. **a, b** The coupled CESM and **c, d** GFDL CM experiments. The left panels show the low-resolution models minus ERA-Interim, the right panels the high-resolution models minus ERA-Interim. Contour interval of 0.2 m/s. Color bars at bottom apply to all panels

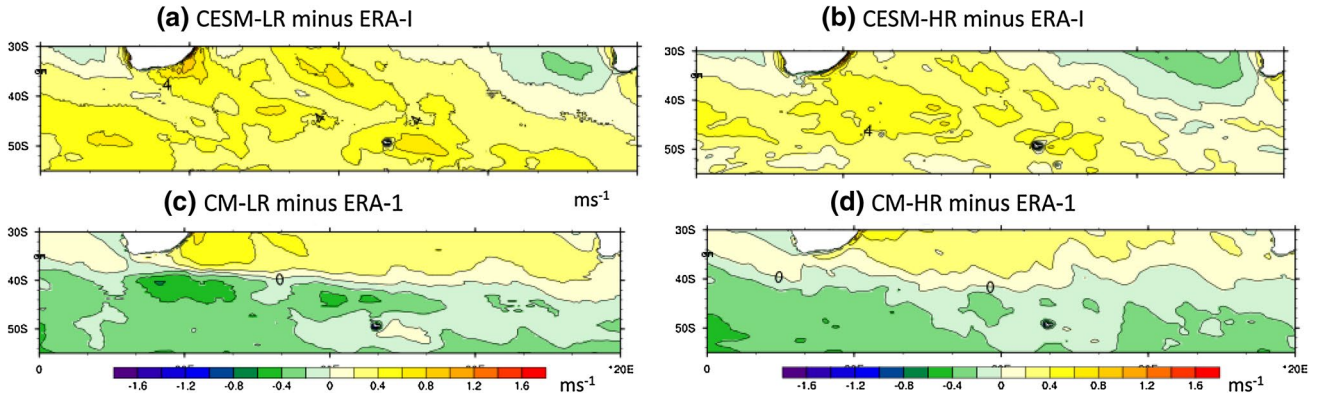

Fig. 6 As Fig. 5 but for DJF in the South Indian Ocean

to ocean resolution in June–July–August (JJA), time of the strongest Southern Hemisphere storm track, is similar to that in DJF for GFDL-CM, whilst the response in CESM is slightly stronger than in DJF: but again at 850 hPa there is very weak sensitivity in both models (not shown).

3.3 Comparison with reanalysis data

The model results are now compared against ERA-Interim Reanalysis (ERA-I: Dee et al. 2011), regridded from its native spectral T255 resolution onto a similarly spaced 0.75° regular grid. As with the climate models, the surface storm track is obtained by daily differencing of the meridional 10 m winds, with data taken from the recent 2003–2016 period.

The surface storm track in CESM is stronger than that in ERA-I at both resolutions, typically by 0.6 m/s or more in the N. W. Atlantic (Fig. 5a, b) and N. W. Pacific (Supp. Fig. 1) and by 0.4 m/s or more in the S. Indian Ocean (Fig. 6a, b). This is partly due to the low level wind bias of CESM discussed in Sect. 3.1, and also due to a general warm SST bias in mid to high latitudes in CESM (Small et al. 2014b).

In the N. W. Atlantic CESM-LR is stronger than ERA-I by more than 1.6 m/s off the US Eastern Seaboard (Fig. 5a). The differences are much reduced in CESM-HR (Fig. 5b) as expected from Fig. 2a but still reach 1 m/s. In the N. W. Pacific, the differences are also reduced in CESM-HR east of Japan (Supp. Fig. 1a, b). Meanwhile in the S. Indian Ocean, there are only subtle changes between resolution in the comparison with ERA-I (Fig. 6a, b), as to be expected from Fig. 4a.

Contrasting with CESM, GFDL-CM has a generally weak storm track compared to ERA-I by 0.4 m/s or more in the N. Hemisphere (Fig. 5c, d; Supp. Fig. 1c, d). In the N.W. Atlantic it is especially apparent in the Gulf Stream region (Fig. 5c, d) and as expected from Fig. 2c, it does not vary much between resolutions. It is a similar story in the N. W. Pacific (Supp. Fig. 1c, d). However, in the S. Indian ocean there is a sensitivity to resolution: GFDL-CM-LR has a much stronger dipole of differences centered approximately along 40°S (Fig. 6c) than seen in GFDL-CM-HR (Fig. 6d). The sign of the dipole difference in GFDL-CM-LR (Fig. 6c) implies that the storm track is located too far to the north compared to ERA-I: the correction made by increasing resolution (seen in Fig. 4c) is opposite-signed and strengthens the storm track south of 40°S and weakens it further north.

These results show that both high resolution CESM and CM correct the storm track towards reanalysis values in the key regions where they also show large differences with low-resolution (in the N. Hemisphere in CESM, in the S. Ocean in GFDL-CM). However, as large overall biases remain, the next sub-section considers a cleaner assessment of the models.

3.4 CESM: comparison with an atmosphere-only model run

As noted above in Sect. 3.1, the boundary layer scheme used in the CESM simulations produces a too strong surface storm track at all resolutions, as seen in Figs. 5 and 6 and Supp. Figure 1. This global boundary layer bias problem complicates interpretation of local changes with resolution, and therefore a comparison is also made with an atmosphere-only simulation made with the CESM model with observed SST (comparable simulations with the GFDL-CM atmosphere model were not readily available). Differences between the coupled models and this atmosphere-only model will be mainly due to the different SST, and the presence or absence of coupling: but not due to differences in model physics or the influence of data assimilation.

The CESM1 atmosphere-only run, with the same atmosphere model version as in the coupled run, and with 0.25° resolution, is used as a "reference" run here. It uses observed, daily 0.25° SST (Reynolds et al. 2007) as the surface boundary condition, for the period 2003–2009 (see Table 1 for details) and the run is referred to as CESM-A. As daily 10 m wind data was not saved in CESM-A, the model bottom layer (with mid-level at about 60 m) wind variability is compared with the same in CESM-LR and CESM-HR. The results are shown as near -surface storm track in the CESM coupled model minus that in the CESM-A, for the North Atlantic and North Pacific (Fig. 7). (Statistical significance is not assessed for this comparison as the CESM-A run is short—a total of 14 years.) Off the US east coast, the storm track in CESM-LR is stronger than in CESM-A by up to 0.8 m/s (Fig. 7a) and is also stronger east of Japan, by 0.4–0.6 m/s (Fig. 7c). This occurs in the same regions where CESM-HR has significantly reduced storm track magnitude compared to CESM-LR (Figs. 2, 3), and thus there is a reduction in the bias with high resolution in both regions as confirmed by Fig. 7b, d. There is not a perfect match between CESM-HR and CESM-A (see Fig. 7b, d) but the differences are generally much smaller in absolute magnitude than with CESM-LR. This analysis shows that CESM-HR has a more realistic storm track than CESM-LR (relative to simulations forced with observed SSTs), and hence the reduction of storm track strength with resolution corresponds to a reduced bias, at least locally, confirming the results of Sect. 3.3. The following section aims to explain why the storm track is sensitive to ocean model resolution.

4 What governs the storm track response to resolution?

We have illustrated the differences of storm tracks with increased ocean resolution in the CESM and GFDL CM and showed a lack of coherent large-scale increase in storm activity in the high-resolution simulations, despite the better resolved ocean mesoscales. To better understand what drives the storm track sensitivity to resolution we focus, in the following, on changes in surface temperature and changes in atmospheric processes that relate to storm tracks.

4.1 Model SST bias, and sensitivity of mean SST and surface temperature gradient to resolution

Several aspects of the mean state of the climate model can affect the storm track activity. For example, the CESM simulation with a low-resolution ocean exhibits too-warm water off the U.S. east coast over the continental shelf, and too cold water in the central North Atlantic, relative to observations (Fig. 8a). The latter is partly due to errors in the Gulf Stream path (i.e. the absence of the Northwest Corner and thus too southerly and zonal position of the North Atlantic Current, which leads to waters that are too cold at the surface between 40°N and 50°N and around 40°W: Weese and Bryan 2006). On the other hand, the former is due to overshooting of Gulf

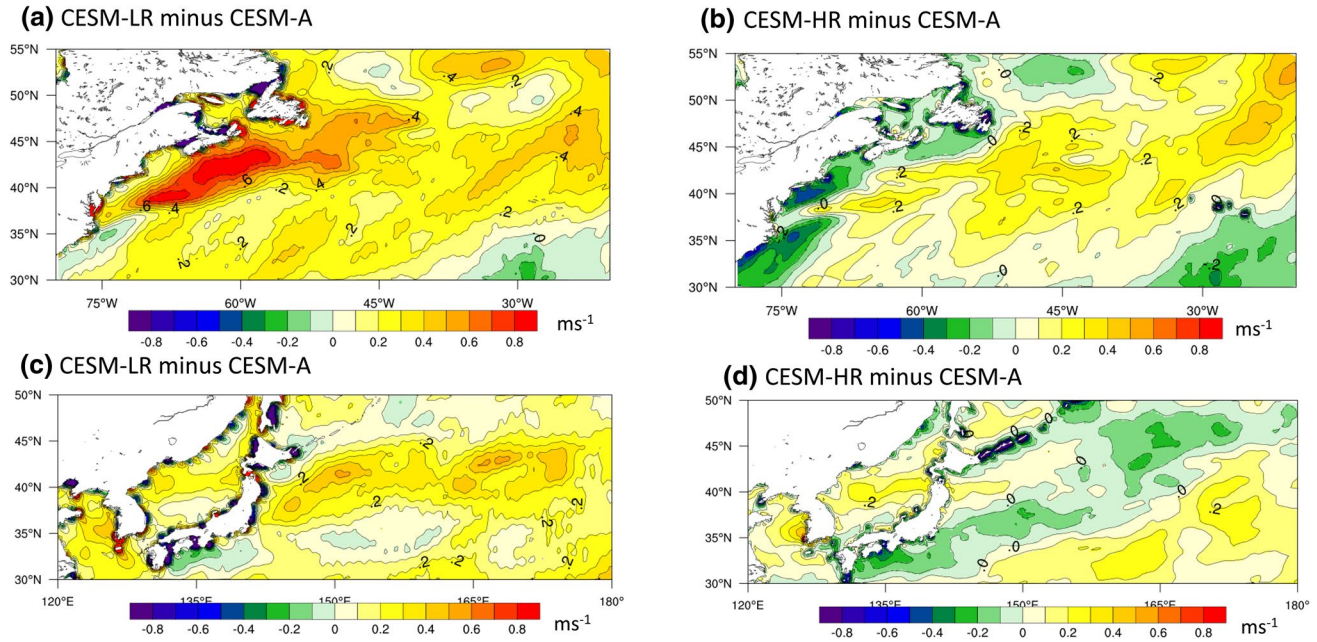

Fig. 7 Difference between near-surface storm track in coupled CESM experiments and atmosphere-only CESM-A (all with the same atmosphere model and resolution), for DJF in the **a, b** North-West Atlantic and **c, d** North-West Pacific. The left panels show CESM-LR minus CESM-A, the right panels CESM-HR minus CESM-A. Contour interval of 0.1 m/s

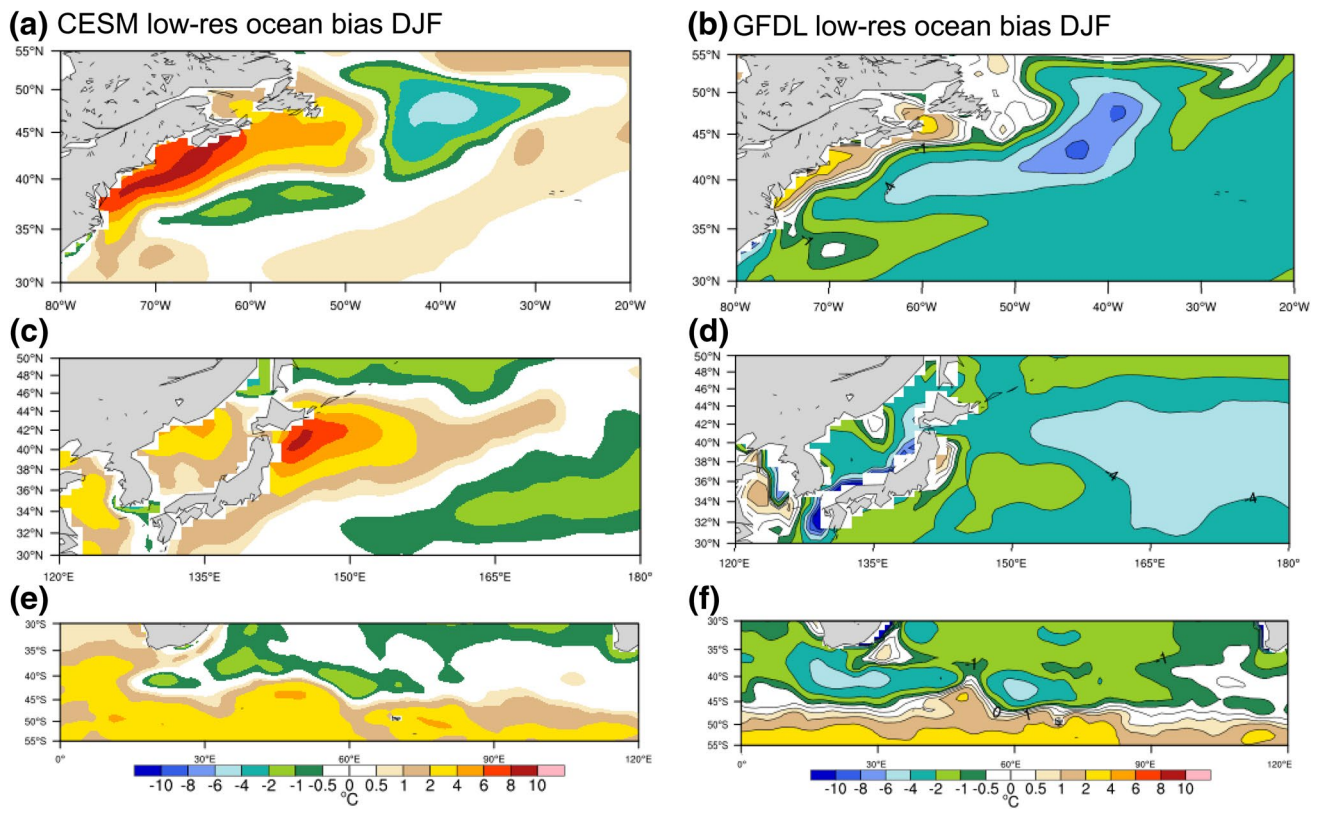

Fig. 8 Difference between model SST and observed SST (HadISST; Hurrell et al. 2008), for DJF. **a, c, e** are for CESM-LR and **b, d, f** are for GFDL-CM-LR. **a, b** for North-West Atlantic, **c, d** for North-West Pacific, **e, f** for S. Indian Ocean. The color bar at bottom applies to all panels

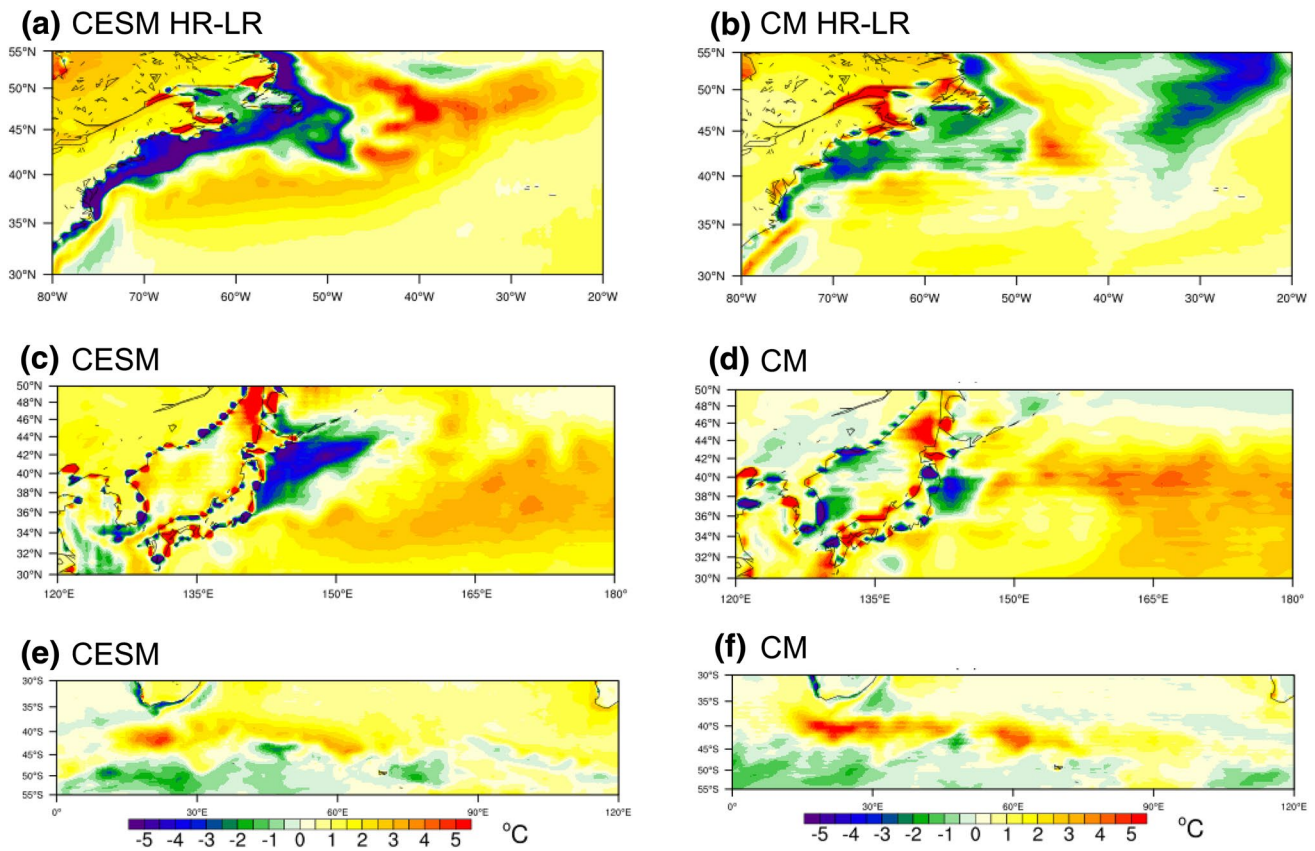

Fig. 9 As Fig. 8 but now showing difference in surface temperature between high-resolution model and low-resolution version, in DJF. The color bar at bottom applies to all panels

Stream which impinge on the U.S. northeast shelf, while the observed Gulf Stream separates near Cape Hatteras. This is one of the most common and longstanding limitation of the low-resolution climate models, including various CESM (e.g. Danabasoglu et al. 2012) and CMIP5 (e.g. Booth et al. 2017) models.

Using a high-resolution ocean component leads to a dramatic improvement in the midlatitude North Atlantic SST (see Small et al. 2014b), removing much of the large-scale biases, due to the better resolved Gulf Stream. This can be seen by comparing Fig. 9a (CESM-HR minus CESM-LR) and Fig. 8a (CESM-LR minus observed SST): opposing colors in the two maps in the Gulf Stream vicinity imply improvements with resolution.

The GFDL models exhibit different SST bias behavior. The low resolution model GFDL CM-LR has a dominant cold bias in the Northwest Atlantic (Fig. 8b), and, indeed, over much of the subtropical N. Hemisphere (Vecchi et al. 2014; as found in many CMIP5 models; see Wang et al. 2014), while the warm bias is confined over the continental shelf (Fig. 8b). The cold bias is exacerbated by the absence of the Northwest Corner as in CESM, which in turn is related to inadequate representation of deep overflows and deep western boundary currents (Delworth et al. 2012; Griffies et al. 2014; Saba et al. 2016).

Despite the different SST bias patterns of the low resolution GFDL CM compared to CESM, the change in SST related to increased ocean resolution in GFDL CM (Fig. 9b) is qualitatively similar to that in CESM in the Northwest Atlantic. GFDL CM-HR acts to cool the coastal shelf waters and to warm the south and east, but the SST difference values are much weaker than in CESM (compares Fig. 9a, b). Griffies et al. (2014) found that the effect of resolved eddies in GFDL-CM-HR was to transfer heat upwards and generally warm the surface compared to GFDL-CM-LR: this particularly occurs in the subtropical gyres (see Fig. 9b and also Fig. 5 of Griffies et al. 2014): however, a large region centered around 25°W, 55°N in the subpolar gyre cools considerably in GFDL-CM-HR (Fig. 9b), for reasons unknown.

The CESM and GFDL CM with the high-resolution ocean also improve upon SST biases in the North Pacific and southern Indian Ocean. In the North Pacific high resolution acts to cool the region east of Japan (Fig. 9c, d), which has a warm SST bias in the low resolution case (Fig. 8c, d), especially in CESM, but further east the high-resolution models are warmer.

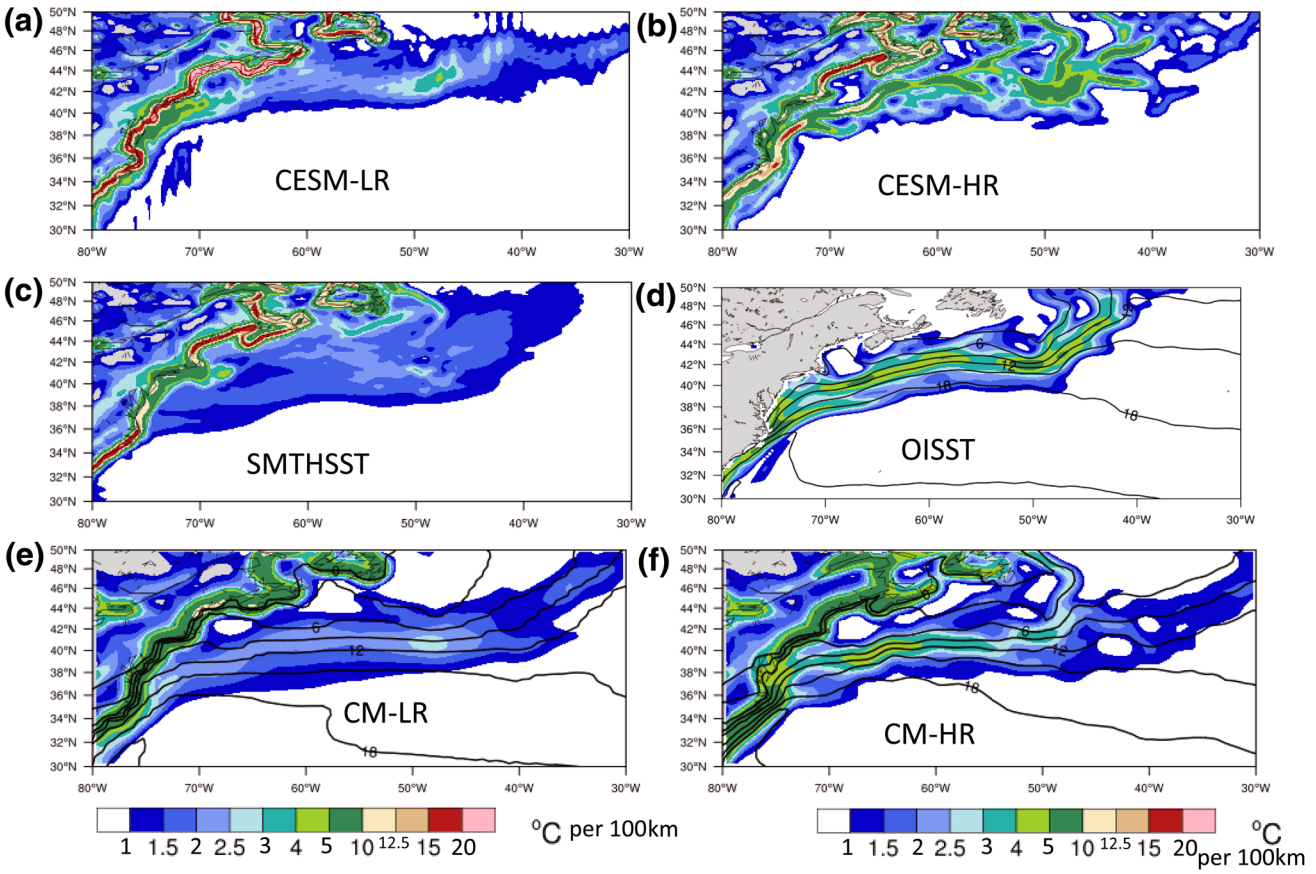

Fig. 10 Surface temperature gradients in DJF (magnitude of the gradient of the mean temperature, in °C per 100 km). The color bar is non-uniform and shown at bottom. **a**–**c** from CESM, **d** from Reynolds et al. (2007) SST, **e, f** from GFDL-CM. Contours of surface temperature are shown on **d**–**f**. For all panels except **d** the surface temperature over land is included in the calculation

In the southern Indian Ocean/Agulhas Return Current region, the low-resolution models exhibit a dipole of cold bias equatorward of warm bias (Fig. 8e, f), which is partly due to weak frontal gradients. In addition, Weijer et al. (2012) noted that the Agulhas Retroflection was too weak, with too much leakage of Indian Ocean waters into the Atlantic, in CCSM4, which had the same ocean resolution as CESM-LR: this is likely also true in GFDL-CM-LR, and would contribute to the cold bias region in Fig. 8e, f. Again, the globally cool nature of GFDL-CM-LR (Vecchi et al. 2014) exacerbates the cold bias in this region (Fig. 8f). The sharpening of the SST gradient and presence of more realistic Agulhas Retroflection in the high-resolution models leads to large improvements upon the low resolution (Fig. 9e, f, compare to Fig. 8e, f). This is most notable in GFDL-CM-HR (Fig. 9f) and we suggest below that this fact explains the stronger sensitivity of storm track in this region to ocean resolution in the GFDL CM suite than in CESM.

An important consequence of the reduction of warm coastal SST bias in the high-resolution model (particularly CESM; Fig. 9a) is the change to land–sea temperature contrast. This is perhaps best seen in full fields of the surface temperature gradient, including data from land and ocean, from CESM-HR and CESM-LR in the Northwest Atlantic in Fig. 10. The low-resolution ocean case has an overly strong horizontal surface temperature gradient (which is associated with the warm bias in the coastal ocean), all along the coastline from Florida northwards (Fig. 10a), stronger and more coherent than that seen with the high-resolution ocean (Fig. 10b). This is also seen as cold colors along the coastline in the difference map of Fig. 11a below. Close inspection reveals that the difference in surface temperature gradient along the coast is typically 9 °C per 100 km to 15 °C per 100 km (Supp. Fig. 2).

The reduced surface temperature gradient at the coastline in CESM-HR is, however, countered by the stronger SST gradient offshore over the better resolved Gulf Stream (Fig. 10b, and warm colors in Fig. 11a). In fact in CESM-HR, the magnitude of the gradient of the time-mean SST in DJF over the Gulf Stream reaches 10 °C per 100 km to 20 °C per 100 km (Fig. 10b), which is much stronger than observed in the satellite observation based 0.25° NOAA OI SST (Reynolds

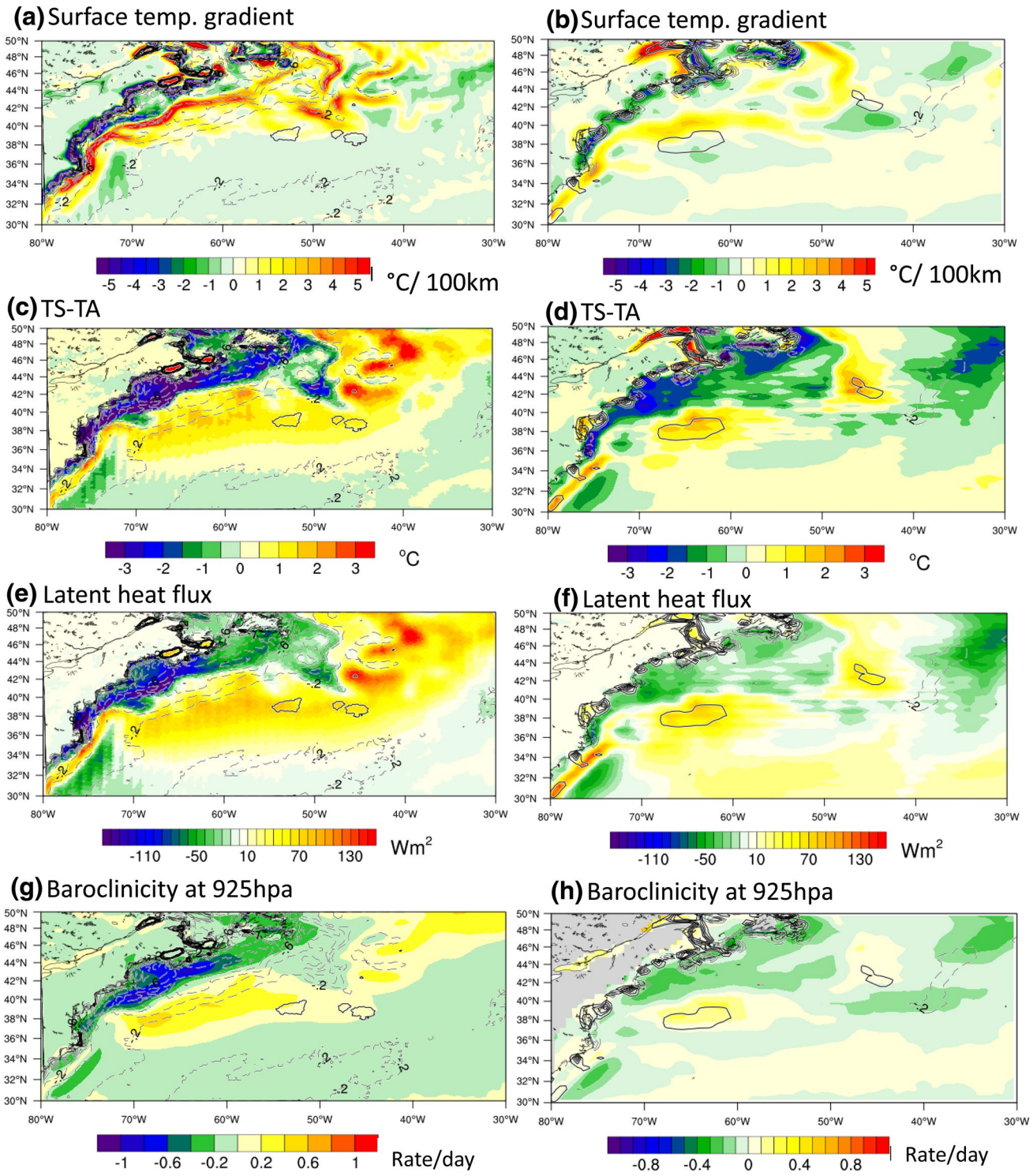

Fig. 11 Near surface factors (as labelled) affecting storm track strength off US East coast in DJF. Left panels: CESM-HR minus CESM-LR. Right panels: GFDL-CM-HR minus GFDL-CM-LR. Overlaid are 10 m storm track differences, with a 0.2 m/s interval. Positive values are solid, negative dashed, and the zero contour is omitted

et al. 2007) where it is typically less than 10 °C per 100 km (Fig. 10d). In CESM-LR, the SST gradient due to the Gulf Stream is weaker than that in CESM-HR by typical values of 5 °C per 100 km to 11 °C per 100 km (Fig. 11a, Supp. Fig. 2). Thus the magnitude of the SST gradient weakening seen in CESM-LR is somewhat less than the strengthening of

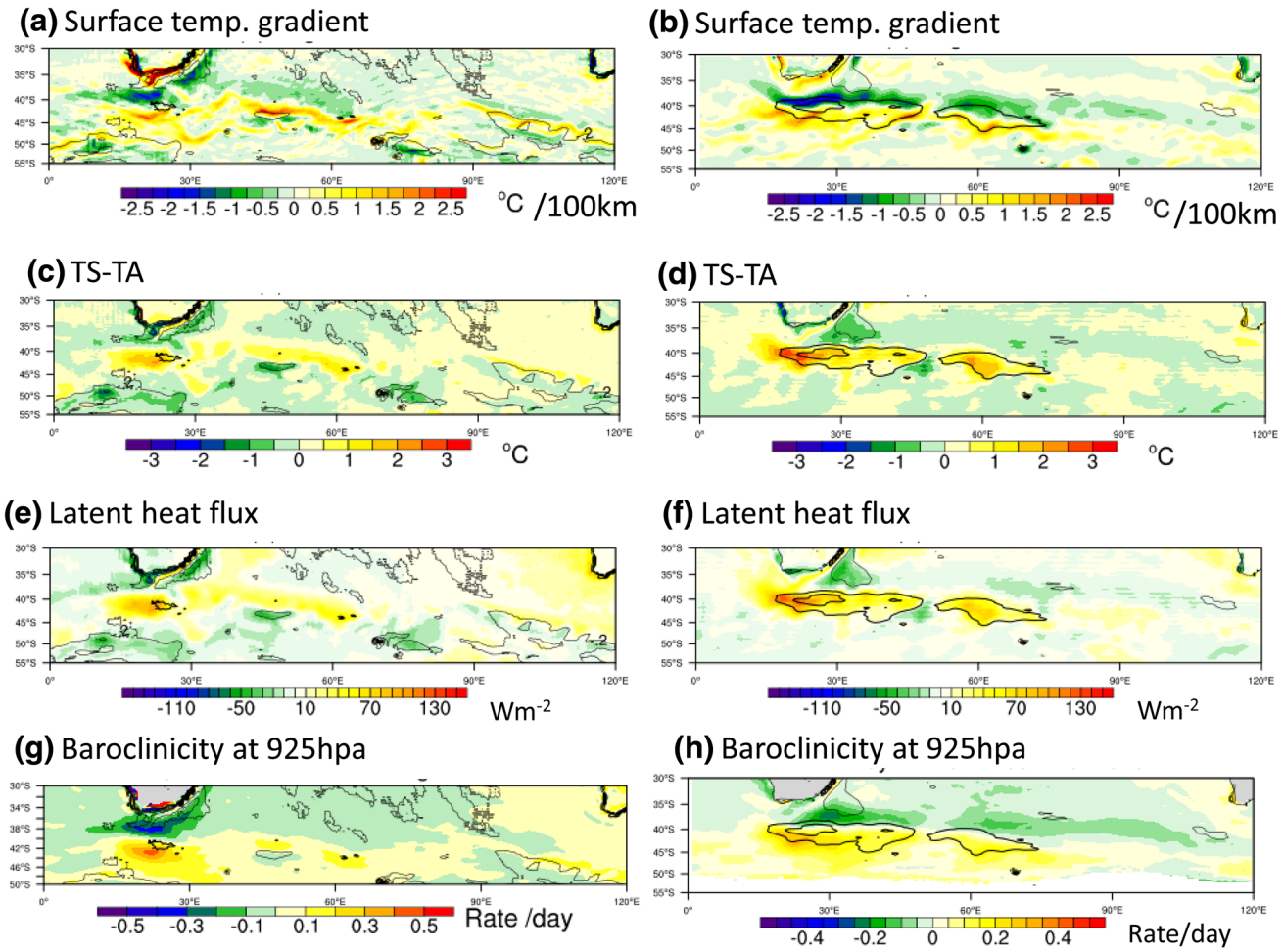

Fig. 12 As Fig. 11 but for South Indian Ocean in DJF. Overlaid are 10 m storm track differences, with a 0.2 m/s interval. Negative values are shown as thin lines here

the land–sea temperature gradient in CESM-LR discussed in the previous paragraph.

Meanwhile, GFDL-CM has weaker gradients along the coastline at both resolutions compared to CESM (Fig. 10e, f), and the strength of the SST gradient along the Gulf Stream in CFDL-CM-HR is more comparable with OISST (Fig. 10f). Overall, the difference in surface temperature gradients between resolutions in GFDL-CM (Fig. 11b) is much weaker than in CESM (Fig. 11a).

The relevance of the land-sea contrast and the ocean SST gradient is discussed below in the context of baroclinicity estimates, and related to the storm track changes. Note that in Figs. 11 and 12, the corresponding differences in surface storm track are overlaid as line contours to aid interpretation.

4.2 Changes to air–sea stability, surface latent heat flux and baroclinicity

The cold air coming off the North American continent in the low-resolution ocean case (CESM-LR) meets the warmer Gulf Stream water immediately offshore leading to a very unstable air-sea interface. In this case, the air-sea temperature difference ΔT is large (> 5 °C) close to the coast, whereas for CESM-HR, large values of ΔT only occur further offshore over the core of the Gulf Stream (not shown). This results in a more stable condition near the coast in CESM-HR (i.e. more negative ΔT; Fig. 11c). Consequently, the turbulent heat flux out of the ocean is smaller over coastal waters in the high-resolution ocean case

(Fig. 11e). Note that for both air-sea stability measured by ΔT (Fig. 11c) and latent heat flux (Fig. 11e), there is an increase of the quantity in CESM-HR further offshore, but the magnitude is generally weaker than that of the coastal reduction.

The atmospheric baroclinicity, or the maximum Eady growth rate, is often used to quantify the effect of mean atmosphere temperature gradients on storm tracks (Eady 1949; Hoskins and Valdes 1990). Free-troposphere values of baroclinicity are most often used to indicate potential storm growth (e.g. Hoskins and Valdes 1990), but it has also been argued that near-surface baroclinicity is important (Nakamura 2004). We computed the baroclinicity at various levels from 950 to 700 hPa. At higher levels the CESM-HR minus CESM-LR difference in baroclinicity exhibited a weak increase in the North Atlantic, but at 925 hPa the change in baroclinicity (Fig. 11g) displays a close resemblance to the storm track difference (Fig. 2a, b) with a dramatic weakening near the coast and a some strengthening closer to the Gulf Stream extension.

Further investigation showed that the reduction in Eady Growth rate in coastal waters at 925 hPa was dominated by the change in vertical stability (buoyancy frequency) and not by the change in horizontal temperature gradient, the latter being more important outside of the boundary layer. This contrasts with some results from AMIP runs with smoothed SST in the North Atlantic (Small et al. 2014a), but is consistent with AMIP simulations of the North Pacific (Kuwano-Yoshida et al. 2017) where the change in stability is also the major factor.

The above results indicate that the time-mean SST difference between CESM-HR and CESM-LR is most important in setting the difference in surface storm track in the Northwest Atlantic as defined by meridional wind variability. SST gradients appear to be less important, as these are much stronger in CESM-HR, but the surface storm track differences are predominantly negative. Part of the reason for this is that the enhanced SST gradient in CESM-HR is countered by a more reduced land-sea surface temperature gradient.

The corresponding differences in the above "storm-track-forcing" metrics between GFDL-CM-HR and GFDL-CM-LR in the North Atlantic have similar spatial structure to CESM, but are generally much weaker (Fig. 11b, d, f, h). This explains the weaker storm track sensitivity to resolution in this region in GFDL CM, consistent with the difference in mean SST shown in Fig. 9b.

The metrics were also computed for the North Pacific (Supp. Fig. 3) where similar reductions in the storm-track-forcing metrics were seen off the Japan coast. Meanwhile, in the southern Indian Ocean in DJF (Fig. 12) and in JJA (Supp. Fig. 4), it was found that GFDL CM showed the larger differences in air-sea stability between resolutions (Fig. 12d), compared to CESM (Fig. 12c), likely leading to the stronger storm track response in GFDL CM in this region (Fig. 4a, c). Here, air-sea stability differences between resolutions (Fig. 12c, d), as well as latent heat flux differences (Fig. 12e, f), better matched the spatial distribution of storm track change (Fig. 4a, c) than did surface temperature gradient (Fig. 12a, b, g). Further, as in the N. Atlantic, the pattern of boundary layer baroclinicity difference (Fig. 12g, h) appears to be more constrained by stability difference and hence stratification difference, than by changes in surface temperature gradient (Fig. 12a–d).

5 Alternative metrics of the storm track

So far the paper has focused on one commonly used metric of the storm track, namely the synoptic variability of meridional wind. In this section alternative metrics are presented, both Eulerian and Lagrangian.

5.1 Eulerian measures

A key aspect of synoptic variability in midlatitude regions is precipitation. A substantial portion of the mean precipitation of the season occurs in atmosphere fronts associated with synoptic storms (Catto et al. 2012). These storms regularly develop and grow near the western boundary currents, where their precipitation rates are affected by the underlying SST field (Czaja and Blunt 2011; Parfitt and Czaja 2016; O'Neill et al. 2017).

For reference the time-mean fields of total monthly precipitation rate for the Northwest Atlantic and Northwest Pacific in DJF from the high-resolution models are shown in Fig. 13. The now-familiar band of strong precipitation along the Gulf Stream can be seen, maximizing downstream of the coast (Fig. 13a, c; Minobe et al. 2008, 2010; Czaja and Blunt 2011; O'Neill et al. 2017). Likewise, precipitation is maximized east of Japan (Fig. 13b, d). CESM has more precipitation than GFDL CM, and indeed CESM-HR has a positive precipitation bias when compared to GPCP observations (Small et al. 2014b).

The contrasts between high-resolution and low-resolution precipitation are shown in Fig. 14. In general, these maps have more equal amplitudes of positive and negative anomalies than the corresponding surface meridional wind difference plots (Figs. 2, 3). In the North Pacific in both models, and in the North Atlantic in CESM, precipitation variability is enhanced in the high-resolution cases, except close to the U.S. northeast coast and the Japan east coast. The positive anomalies represent not just a shift of precipitation away from the coast, but also an absolute increase in the maximum precipitation rates over the ocean front: by at least 1mm/day, and between 10 and 15% increase, for the N. Atlantic in CESM (not shown). The weakest change

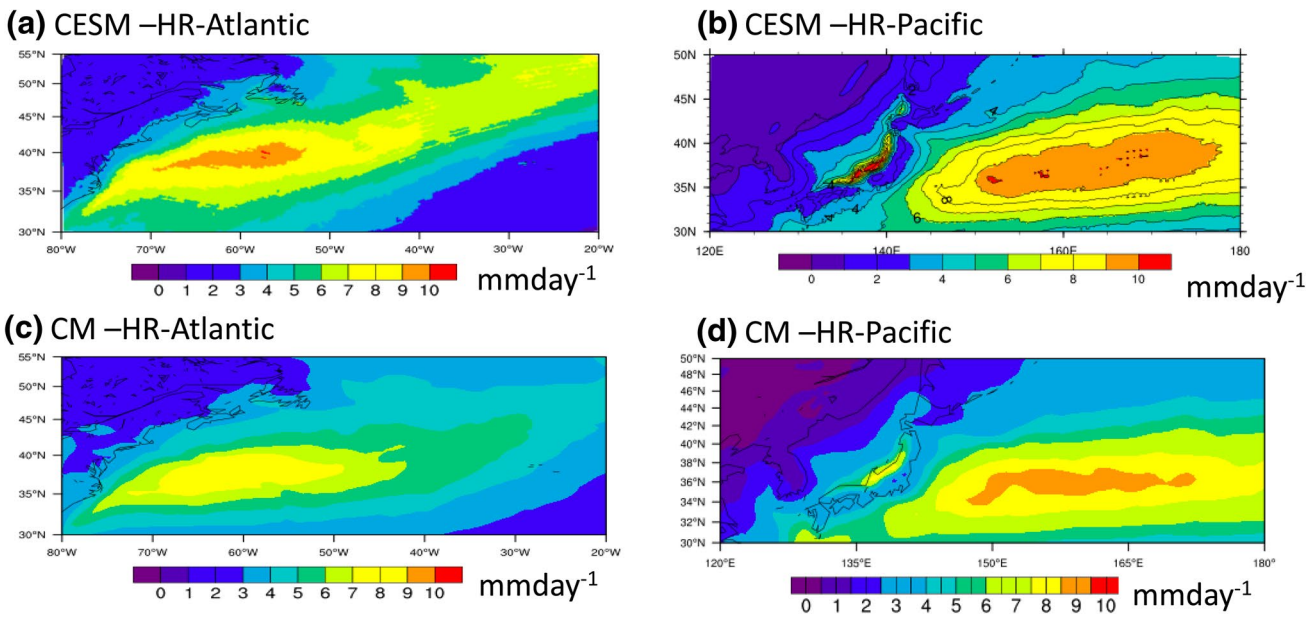

Fig. 13 Climatological precipitation fields in DJF in high-resolution models. **a** CESM-HR N. Atlantic, **b** CESM-HR N. Pacific, **c** GFDL-CM-HR N. Atlantic, **d** GFDL-CM-HR N. Pacific

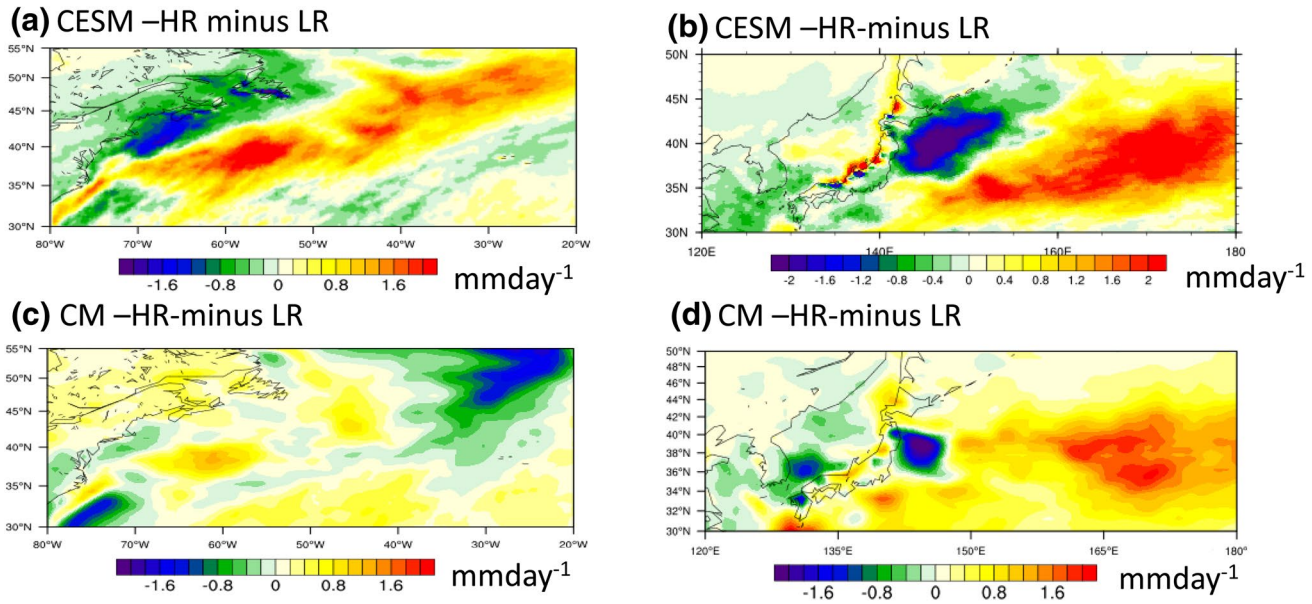

Fig. 14 As Fig. 13, but now showing the precipitation difference between high-resolution and low-resolution models

over the ocean front is in GFDL CM in the North Atlantic (Fig. 14c). All four panels of Fig. 14 bear a close correspondence to the change in SST with resolution shown in Fig. 9a–d, confirming the strong control of SST on the precipitation field in these regions. The amplification of the positive pole of the differences in these precipitation fields, compared to the surface wind fields, may be due to the non-linear response of atmosphere moisture to SST given by the Clausius–Clapeyron equation, with disproportionally large precipitation responses to warm SST anomalies. It is also noted here that not just the mean, but the synoptic variability of precipitation, and also of latent heat flux, an important contributor to precipitation, has a similarly enhanced positive anomaly (not shown) compared to the meridional wind storm track differences.

5.2 Lagrangian storm track

The Eulerian storm track estimates given above, based on variances of synoptic-timescale filtered quantities, do not distinguish between changes to storm intensity versus changes to path and frequency of storms. It would be useful to know these quantities, particularly with respect to quantifying U.S. east coast storms and storms off Japan which may impact the mainland. To address this, a Lagrangian approach is taken using the CESM model, based on identification of surface pressure minima, as described in Sect. 2.2.

The Lagrangian storm track density (number of storms per year in a $6° \times 6°$ grid box) in CESM-HR in DJF reveals the expected maxima in the central North Pacific and North Atlantic (Fig. 15a). The Atlantic maxima is somewhat further downstream than that shown in e.g. Hoskins and Hodges (2002), although this is primarily due to the fact that the method used here requires a cyclone to have a surface pressure less than 980 hPa for at least 6 h during its lifetime for inclusion. Plots using weaker cutoffs reduce this downstream shift by including storms earlier (more westward) in their lifetime (not shown). The mean surface pressure over the ocean [equal to sea level pressure (SLP) by definition] at each spatial location for all storms is shown in Fig. 15c. This is similar in spatial pattern to the climatological mean SLP distribution, but has lower SLP because only low pressure cyclones are included.

The annual track density difference between CESM-HR and CESM-LR models (storms stronger than 980 hPa only), is shown in Fig. 15b. Compared to the Eulerian quantity of CESM-HR minus CESM-LR difference in 850 hPa meridional winds (Figs. 2b, 3b), some similarities between Lagrangian and Eulerian approaches are apparent, such as a reduction in track density off Japan where the Eulerian variance of wind is reduced, combined with a corresponding increase to the east. Some differences between the techniques exist as well. Track density changes are relatively small along the U.S. east coast between the two resolutions, contrasting with the notable reduction in the Eulerian quantity. However, it should be noted that a similar shift to that seen in Fig. 2b is noticeable further north in the Atlantic basin with decreased storm activity off the coast of Newfoundland (and shift further offshore) with CESM-HR.

Low pressure storms are weaker (i.e. higher SLP, warm colors) in CESM-HR off the Japan coast, and stronger (blue colors) in the central North Pacific (Fig. 15d), again consistent with the Eulerian wind quantities. This response is not as noticeable off the U.S. east coast, which shows deeper SLP immediately adjacent to the coast in CESM-HR (Fig. 15d) and weak, positive values further offshore, although as before, storms are weaker along the Canadian coast and the closer one gets to the core of the North Atlantic storm track region. Since Lagrangian analyses are most robust for mature, deep cyclones, this implies that many of the changes seen directly off the U.S. coast in the Eulerian metrics may be primarily centered around storms in the nascent phase. The stronger agreement in the North Pacific, on the other hand, indicates that storm track differences are robust across with regard to both storm frequency and intensity.

The Lagrangian track density analysis shows the N. Pacific storm density in CESM-HR is larger than the N. Atlantic (Fig. 15a). This differs from the Eulerian surface storm, in which the N. Atlantic is stronger than the N. Pacific (Fig. 1b). Part of the difference can be attributed to the differences in the metrics (e.g. Hoskins and Hodges 2002), however another issue relates to the physics of the surface storm track. In the N. Atlantic, the lower tropospheric stability is weaker than in the N. Pacific, which leads to stronger vertical momentum mixing and a stronger surface storm track (Booth et al. 2017). A separate metric of the mid-tropospheric storm track is the precipitation, which is larger in the N. Pacific than the N. Atlantic (Fig. 13) and therefore consistent with the Lagrangian storm track. Additional comparison of the Lagrangian and Eulerian measures of storm tracks is made in Sect. 6.2 below.

6 Discussion

6.1 On the influence of absolute SST vs. SST gradient

Why does the storm track in the N. Hemisphere in CESM1 not increase in strength when the ocean model produces a much stronger SST gradient? In this model, the increase in SST gradient seen in CESM-HR relative to CESM-LR mainly occurs due to a large cooling of the shelf and adjacent slope waters. In other words, there is an average reduction of spatially-averaged SST under the storm track that accompanies the increase in SST gradient, and thus a reduction of thermodynamic (surface) energy to the atmosphere. This counteracts any increase of storm track due to increased SST gradients. This is consistent with case-studies of Booth et al. (2012) which found that the strength of the storms is more sensitive to the temperature of the SST under the warm sector of the storm than the strength of the SST gradient. In addition to the reduction in absolute SST in the high-resolution CESM, there is a large reduction in land–sea temperature contrast, both factors acting to reduce the storm track activity.

These issues have been addressed in a separate experiment with CESM (referred to here as SmthSST) performed with the same high-resolution components as CESM-HR but where the SST is spatially smoothed before passing to the model coupler where air-sea fluxes are computed (see Ma et al. 2016 for a description of these CESM experiments).

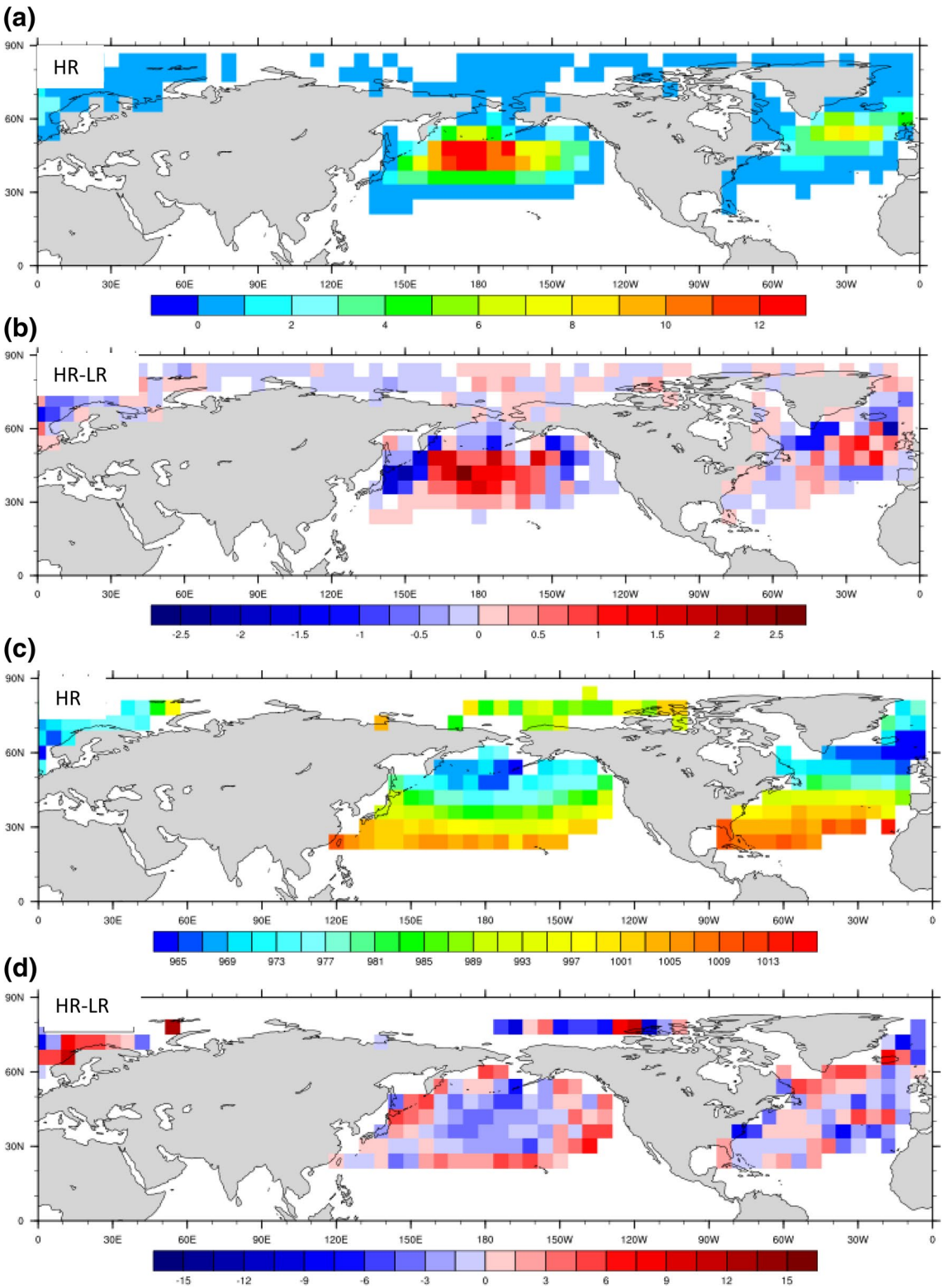

Fig. 15 Lagrangian storm tracks for CESM in DJF. **a, b** Track density. **c, d** Spatial mean SLP for all storms. Full fields for CESM-HR are shown in **a** and **c**: the differences CESM-HR minus CESM-LR are shown in **b** and **d**

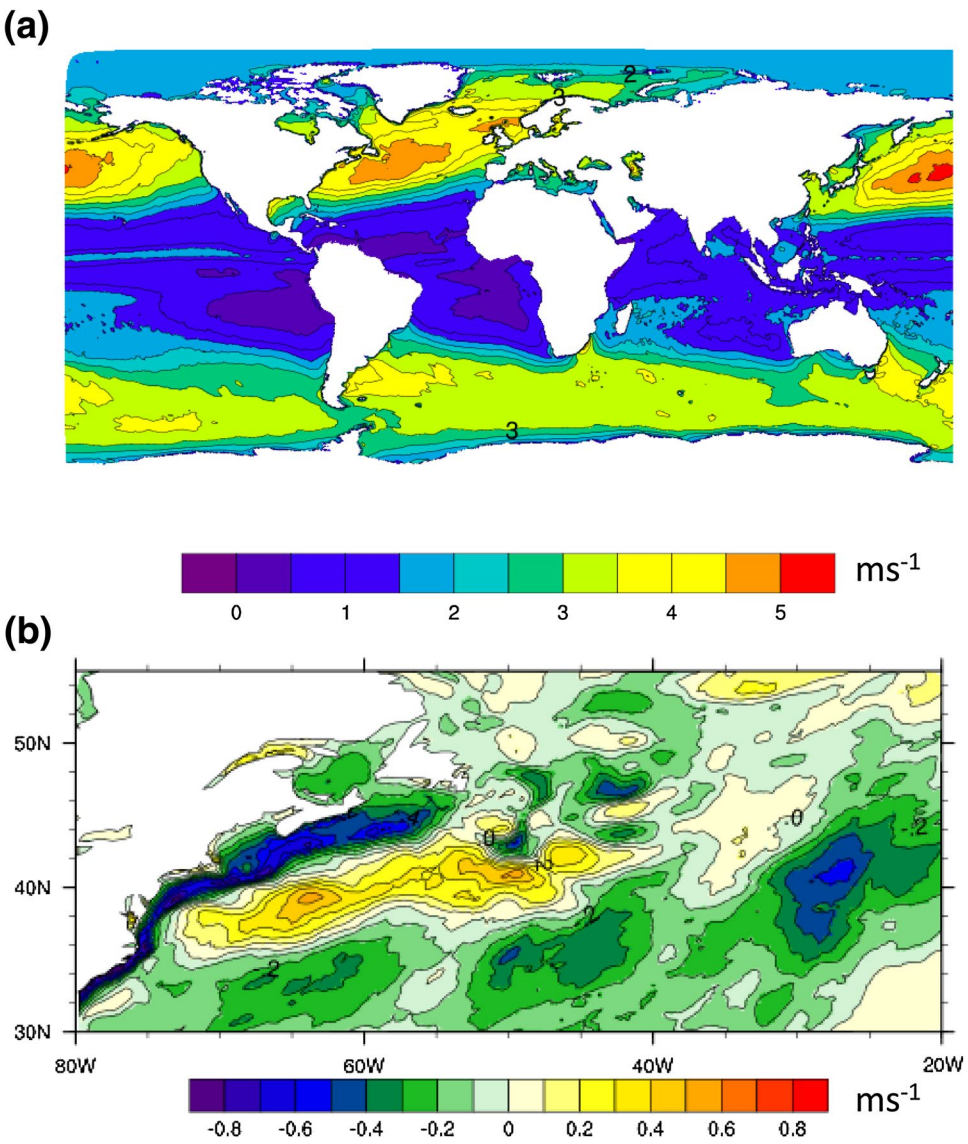

Fig. 16 Result of smoothing SST for air-sea fluxes in a coupled simulation. **a** Surface storm track in SmthSST run, DJF, to compare with Fig. 1b. **b** CESM-HR minus SmthSST differences of surface storm track in the N. W. Atlantic

The motivation here is that by keeping the model components at the same resolution, we are less likely to obtain a very different global solution: but we should see the influence of SST gradients on the atmosphere (and feedbacks to the ocean). Further, changes to SST are made not just primarily on the cold side of the Gulf Stream but more equally on both sides of the ocean front (Fig. 17a). The smoothing was a 1000 km by 1000 km box-car average, which produces a substantially smoother SST field than seen with the 1 degree ocean model (Fig. 10a versus c). The SmthSST simulation is only 10 years long and hence care needs to be taken in assessing the differences from the control CESM-HR run.

Compared against the CESM-HR run (Fig. 1b), the North Atlantic and S. Indian Ocean storm track of SmthSST in DJF is weaker, but the North Pacific storm track is stronger (compare Fig. 16a with Fig. 1b). We believe the N. Pacific storm track difference is affected by large-scale natural variability and the shortness of the run: the time-mean differences of SST between CESM-HR and SmthSST[1] (Supp. Fig. 5) exhibit overall cooling in the Northwest Pacific which affects the storm track strength. Therefore, we focus on the North Atlantic storm track.

Compared to the mainly monopole structure of the model resolution comparison of Fig. 2a, there is more of a dipole structure in the storm track difference (Fig. 16b), with a stronger storm track over the Gulf Stream region in

[1] Strictly, we use the SST that is used to compute air–sea fluxes in the SmthSST case which by design is smoother than the actual ocean SST, see Sect. 2.

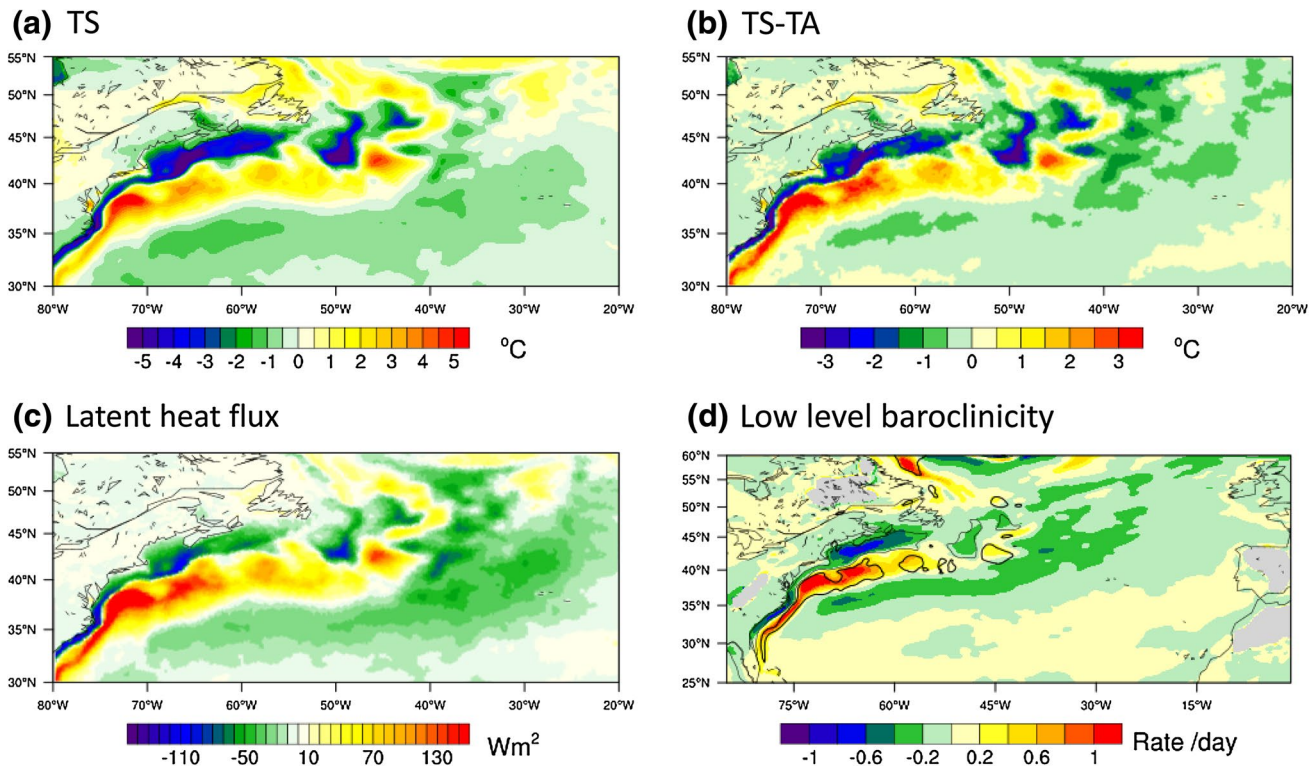

Fig. 17 Result of smoothing SST for air–sea fluxes in a coupled simulation. CESM-HR minus SmthSST differences in storm track forcing metrics in DJF, compare with Fig. 16b. **a** Surface temperature, **b** air–sea temperature difference, **c** latent heat flux, **d** baroclinicity at 925 hPa. **d** shows a larger domain

CESM-HR. SmthSST has weaker surface temperature gradients along the Gulf Stream (Fig. 10c) compared to CESM-HR (Fig. 10b), and also along the coastline compared to CESM-LR (Fig. 10a). Further, the storm track "forcing metrics" also show stronger positive poles in the difference fields (Fig. 17) compared to the model resolution comparison case (Figs. 9a, 11), which illustrates a larger change along the Gulf Stream and hence in the above storm tracks. Further, not only is the storm track stronger in CESM-HR in North Atlantic near the surface, compared to SmthSST, but also in the lower free troposphere at 850 hPa (Supp. Fig. 6).

In the SmthSST case for the North Atlantic, the reduced SST gradient is achieved while keeping the spatial average of SST approximately constant (i.e. roughly equal positive and negative poles of SST difference; Fig. 17a). In this case, an overall increase in spatially-averaged storm track activity can be seen in CESM-HR compared to SmthSST. (This was also seen in Small et al. 2014a where the storm track was increased over large, sub-basin scale regions when the SST was not smoothed, see their Tables 2 and 4.) Also, an overall increase in storm track activity was seen in the southern Indian Ocean in GFDL-CM-HR compared to GFDL-CM-LR, where the main change to SST was an increase in the Antarctic Circumpolar Current region (Fig. 9f), contrasting with the reduction in SST in the U.S. east coast region in the CESM-HR case (Fig. 9a).

These results may help explain the somewhat contradictory results of case studies of single storms described in the Introduction. Sheldon et al. (2017) apply a uniform smoothing everywhere to create their weak SST gradient experiment, whereas Booth et al. (2012) change the gradient by only modifying the SST in the region north and west of the Gulf Stream North Wall. As mentioned above, the latter reduces the overall, spatially-averaged SST whilst the former approximately retains the average SST.

We may also speculate that if the SST gradient is increased in the Northwest Atlantic by artificially increasing SST in the Gulf Stream region (rather than cooling shelf waters), a large and positive response of the storm track could be seen. This may be relevant to future scenarios of climate change, where warming associated with shifts in the Gulf Stream is seen at high-resolution (Saba et al. 2016). It may also have a relevance to the comparison of CESM-HR and GFDL-CM-HR reported in this paper: CESM-HR has much warmer SST in the Gulf Stream region than GFDL-CM-HR, the latter having a large cold bias, and this may be part of the reason why CESM-HR has a much stronger storm track in the Gulf Stream region than GFDL-CM.

6.2 Lagrangian versus Eulerian view of storm track

In Sects. 3 and 4, it was found that the storm track defined in terms of meridional wind variability responded very closely to changes in absolute SST between experiments, causing notable reductions of storm track strength off the east coasts when ocean resolution is increased.[2] However, when different storm track metrics are used, such as mean, or variability of precipitation, or Lagrangian low pressure center tracking, the results are subtly different. For example, precipitation variability was enhanced further downstream from the coast in the high-resolution experiments, possibly as a result of the Clausius–Clapeyron relation, i.e. enhanced sensitivity of moisture to warm SST, or due to the free-troposphere baroclinicity which increased offshore. Further, the Lagrangian storm track statistics gave different results for the storm track off the U.S. east coast compared to that off the Japan coast, contrasting to their similar characteristics in Eulerian statistics. This mainly reflects the fact that the Eulerian storm tracks include variability associated with both high and low pressure systems at all locations, whereas the Lagrangian trackers focus on the behavior of the low pressure storm centers. Likewise, metrics based on precipitation are biased towards the atmospheric fronts associated with low pressure systems. It also implies that storms may be preferentially impacted at different stages of their evolution, particularly in near-coastal regions in the Northern Hemisphere.

Additionally, Lagrangian statistics are most robust with large sample sizes of discrete trajectories, and deep, coherent extratropical cyclone activity is less frequent along coastlines (particular the U.S. east coast) relative to in the heart of the storm tracks over the center of the ocean basins, implying that some discrepancy may be mitigated by larger samples with high-resolution models.

6.3 Role of ocean circulation

This paper has focused on changes of atmosphere storm track induced by refining ocean resolution, via changes in mean SST, but has not attempted to explain in any detail why the mean SST (or variability of SST), changes in the first place. Clearly the different ocean circulation at 0.1° resolution plays a role, such as by improving Agulhas leakage and the Agulhas Return Current, and improving (but not fixing) biases in the separation location of the Gulf Stream and Kuroshio, and the path of the North Atlantic Current. Associated feedbacks with the atmosphere will also be important.

In previous studies the ocean circulation and associated heat transport has been implicated in changing atmosphere heat transport in climate models with an eddy-resolving ocean. For example, Bishop et al. (2015) looked at year to year variability in CESM-HR and found a certain degree of compensation between ocean and atmosphere heat transport, related to the "Bjerknes compensation" idea. Further, Roberts et al. (2016) related improvements in the mean surface heat flux and latent heat flux in their model with a high-resolution ocean to differences in meridional heat transport in the ocean. Meanwhile in GFDL-CM, Griffies et al. (2014) showed that the representation of fine-scale currents and stronger gyre heat transport contributed to overall smaller temperature biases and drifts in ocean heat in GFDL-CM-HR compared to models with coarser ocean resolution. Hence better representation of the ocean circulation at high resolution is important for reducing some of the other ocean and atmosphere biases in these climate models, in addition to surface storm track location errors discussed in this paper.

7 Conclusions

This paper has aimed to classify the sensitivity of the atmosphere storm track to ocean model resolution in coupled models. For two major U.S. global climate models, the difference in ocean model resolution between eddy-resolving (0.1°) and eddy-parameterized (1°) ocean is not sufficient to cause a large change in overall storm track strength in coupled climate models, by some typical Eulerian and Lagrangian measures. However, high ocean resolution does improve the location of the storm track maximum. This is manifested by a reduction of storm track strength off the U.S. and Japanese east coasts at high resolution, particularly in the CESM model. In both of these climate models, the atmosphere model resolution is also high (0.25°–0.5°), so that synoptic atmospheric variability is quite well resolved (Colle et al. 2013; Smirnov et al. 2015; Willison et al. 2013).

The most notable differences in storm track strength in CESM are seen in the Northern Hemisphere off the U.S. east coast and Japan coast. In contrast, in GFDL CM, it is the southern Indian Ocean storm track that is most sensitive to ocean model resolution, although the effect is only in the boundary layer. This is due to the largest differences (between HR and LR) of absolute SST and of air–sea stability in CESM being present in the Northern Hemisphere: whilst in the Southern Hemisphere they are weaker. The converse is true for GFDL CM. Further, the surface latent heat flux and the low level baroclinicity are strongly constrained by the surface stability changes. All these factors affect the storm track, but we do not attempt to separate out their influence here.

[2] In our experiments transient eddy kinetic energy at 850 hPa shows very similar behavior to low level meridional wind variance in CESM.

The sensitivity to SST gradient is much weaker than to absolute SST, as shown by the small influence of the strongest SST gradient of all experiments (gradients of 10–20 °C per 100 km in the North Atlantic in CESM-HR: compared to gradients typically less than 5 °C per 100 km in all other regions) contrasting with the strong effect of absolute SST difference in GFDL CM in the Indian Ocean. However, when considering the surface temperature gradient (including land and ocean temperature), CESM-LR has the largest gradient of all simulations, which occurs along the U.S. east coast. Further, an important result of this paper is that the sensitivity of storm track to model resolution is dependent on the low resolution model mean SST bias and how much it is improved at high resolution.

It was shown that in the same regions where ocean model resolution has biggest impact on storm track strength (N. Hemisphere in CESM: S. Indian Ocean in GFDL-CM), the case with high-resolution is closest to both an atmosphere-only model (forced by observed SST) and ERA-Interim reanalysis data. Further the metrics of Sect. 4 allowed these storm track differences to be robustly attributed to the time-mean SST difference. Thus, although there are difficulties in directly comparing CESM with GFDL-CM and ERA-Interim, because of the different atmosphere physics and impact of data assimilation, these results show that use of a high-resolution ocean model in the coupled system will indeed improve the storm track (at least regionally) provided it improves the mean SST. We did not see evidence that changes to SST variability (such as due to ocean mesoscale) have a big impact on surface storm track: evidenced by the fact that there were minimal changes in the storm track across resolution in the S. Ocean/ACC region in CESM and in the N. Hemisphere storm track in GFDL-CM, despite these being regions of strong eddy activity in the oceans. But for other metrics of storm track such as precipitation, we did see an increase in some of these cases, suggesting a possible role for effects of eddies via diabatic responses in the atmosphere, as suggested by Ma et al. (2015, 2017).

An experiment using high-resolution CESM but with the SST heavily spatially smoothed before being used to compute fluxes showed a weaker storm track in the North Atlantic compared to the standard coupling experiment. This showed that for a sufficiently large change in SST gradient, and when the difference in mean SST is not dominated by a monopole reduction, with its associated change in land-sea contrast, SST gradients can drive a stronger storm track response.

Finally, subtly different results were found for different storm track metrics, showing that care needs to be taken in choosing a metric of most "usefulness." Similar findings were found in a comparison of different Lagrangian methods by Neu et al. (2013). In this paper, we have focused on meridional wind variability which is related to temperature variability at western boundaries.

Acknowledgements An anonymous reviewer is thanked for constructive comments on the paper, especially for suggesting a more detailed assessment against ERA-Interim Reanalysis. CESM1 was a community development effort, as described in Hurrell et al. (2013), for which we are very grateful. The CESM1 simulations described in this paper were performed at NCAR Wyoming Supercomputer Center. We also thank Tom Delworth, Gabriel Vecchi and all the scientists at GFDL who invested time and resources to produce the GFDL CM simulations used in this research. RJS was supported by Department of Energy Office of Biological and Environmental Research, via the Scientific Discovery through Advanced Computing (SCIDAC) project number SC0006743,and National Science Foundation (NSF) Collaborative Research: EaSM-3: Regional decadal predictions of coupled climate-human systems 1419585. Y-OK was supported by NSF Division of Atmospheric and Geospace Science Climate and Large-scale Dynamics Program (AGS-1355339), NASA Physical Oceanography Program (NNX13AM59G), and DOE Office of Biological and Environmental Research Regional and Global Climate Modeling Program (DE-SC0014433). JFB was partially supported by the National Oceanic and Atmospheric Administration (NOAA) Climate Program Office's Modeling, Analysis, Predictions, and Projections program, Grant #NA15OAR4310094. R. Msadek was supported by GFDL and UCAR when the GFDL simulations used in this paper were produced and analyzed. We thank Steve Griffies for helping interpreting the results. Discussions with Hisashi Nakamura, Niklas Schneider and Shoshiro Minobe were very appreciated.

References

Bishop SP, Bryan FO, Small RJ (2015) Bjerknes-like compensation in the wintertime North Pacific. J Phys Oceanogr 45:1339–1355

Booth JF, Thompson L, Patoux J, Kelly KA, Dickinson S (2010) The signature of midlatitude tropospheric storm tracks in the surface winds. J Clim 23:1160–1174

Booth JF, Thompson L, Patoux J, Kelly KA (2012) Sensitivity of midlatitude storm intensification to perturbations in the sea surface temperature near the Gulf Stream. Mon Weather Rev 140:1241–1256

Booth JF, Kwon Y-O, Ko S, Small RJ, Msadek R (2017) Spatial patterns and intensity of the surface storm tracks in CMIP5 models. J Clim 30:4965–4981

Brayshaw DJ, Hoskins B, Blackburn M (2009) The basic ingredients of the North Atlantic storm track. Part I: Land–sea contrast and orography. J Atmos Sci 66:2539–2558

Brayshaw DJ, Hoskins B, Blackburn M (2011) The basic ingredients of the North Atlantic storm track. Part II: Sea surface temperatures. J Atmos Sci 68:1784–1805

Bryan FO, Tomas R, Dennis JM, Chelton DB, Loeb NG, McClean JL (2010) Frontal scale air–sea interaction in high-resolution coupled climate models. J Clim 23:6277–6291

Businger S, Graziano TM, Kaplan ML, Rozumalski RA (2005) Cold-air cyclogenesis along the Gulf Stream front: investigation of diabatic impacts on cyclone development, frontal structure and track. Meteorol Atmos Phys 88:65–90

Catto JL, Jakob C, Berry G, Nicholls N (2012) Relating global precipitation to atmospheric fronts. Geophys Res Letts 39:L10805. https://doi.org/10.1029/2012GL051736

Chang EKM, Lee S, Swanson KL (2002) Storm track dynamics. J Clim 15:2163–2183

Colle BA, Zhang Z, Lombardo KA, Chang E, Liu P, Zhang M (2013) Historical evaluation and future prediction of eastern North American and Western Atlantic extratropical cyclones in the CMIP5 models during the cold season. J Clim 26:6882–6903

Czaja A, Blunt N (2011) A new mechanism for ocean–atmosphere coupling in midlatitudes. Q J R Meteorol Soc 137:1095–1101

Danabasoglu G, Bates SC, Briegleb BP, Jayne SR, Jochum M, Large WG, Peacock S, Yeager SG (2012) The CCSM4 ocean component. J Clim 25:1361–1389

Delworth TL et al (2006) GFDL's CM2 global coupled climate models. Part I: formulation and simulation characteristics. J Clim 19:643–674

Delworth TL et al (2012) Simulated climate change in the GFDL CM2.5 high-resolution coupled climate model. J Clim 25:2755–2781

Dee DP, 35 co-authors (2011) The ERA-Interim reanalysis: configuration and performance of the data assimilation system. Q J R Meteorol Soc 137:553–597

Eady ET (1949) Long waves and cyclone waves. Tellus 1:33–52

Gent PR, McWilliams JC (1990) Isopycnal mixing in ocean circulation models. J Phys Oceanogr 20:150–155

Gent PR et al (2011) The community climate system model version 4. J Clim 24:4973–4991

Griffies SM et al (2014) Impacts on ocean heat from transient mesoscale eddies in a hierarchy of climate models. J Clim 28:952–977

Guo Y, Chang EKM, Leroy SS (2009) How strong are the southern hemisphere storm tracks? Geophys. Res Lett 36:L22806. https://doi.org/10.1029/2009GL040733

Hoskins BJ, Hodges KI (2002) New perspectives on the Northern hemisphere winter storm tracks. J Atmos Sci 59:1041–1061

Hoskins BJ, Hodges KI (2005) A new perspective on Southern hemisphere storm tracks. J Clim 18:4108–4129

Hoskins BJ, Valdes PJ (1990) On the existence of storm tracks. J Atmos Sci 47:1854–1864

Hunke EC, Lipscomb WH (2008) CICE: the Los Alamos sea ice model user's manual, version 4. In: Los Alamos National Laboratory technical report LA-CC-06-012

Hurrell JW, and Coauthors (2013) The community Earth system model: a framework for collaborative research. Bull Am Meteorol Soc 94:1339–1360

Hurrell JW, Hack JJ, Shea D, Caron JM, Rosinski J (2008) A new sea surface temperature and sea ice boundary dataset for the community atmosphere model. J Clim 21:5145–5153

Joyce TM, Kwon Y-O, Yu L (2009) On the relationship between synoptic wintertime atmospheric variability and path shifts in the Gulf Stream and the Kuroshio extension. J Clim 22:3177–3192

Kuo Y-H, Reed RJ, Low-Nam S (1991) Effects of surface energy fluxes during the early development and rapid intensification stages of seven explosive cyclones in the western Atlantic. Mon Weather Rev 119:457–475

Kuwano-Yoshida A, Minobe S (2017) Storm-track response to SST fronts in the Northwestern Pacific in an AGCM. J Clim 30:1081–1102

Kuwano-Yoshida A, Minobe S, Xie S-P (2010) Precipitation response to the Gulf Stream in an atmospheric GCM. J Clim 23:3676–3698

Large WG, Yeager SG (2009) The global climatology of an interannually varying air–sea flux data set. Clim Dyn 33:341–364

Lawrence DM et al (2011) Parameterization improvements and functional and structural advances in version 4 of the community land model. J Adv Model Earth Syst 3:2011MS000045

Liu WT, Tang W (1996) Equivalent neutral wind. JPL Publication 96-17. http://www.ntrs.nasa.gov/archive/nasa/casi.ntrs.nasa.gov/19970010322.pdf

Liu JW, Zhang S-P, Xie S-P (2013) Two types of surface wind response to the East China Sea Kuroshio Front. J Clim 26:8616–8627

Lorenz DJ, Hartmann DL (2001) Eddy-zonal flow feedback in the Southern Hemisphere. J Atmos Sci 58:3312–3327

Ma X, co-authors (2016) Western boundary currents regulated by interaction between ocean eddies and the atmosphere. Nature 535:533–537

Ma X, Chang P, Saravanan R, Montuoro R, Hsieh J-S, Wu D, Lin X, Wu L (2015) Distant influence of Kuroshio eddies on North Pacific weather patterns. Sci Rep 5:17785 https://doi.org/10.1038/srep17785

Ma X, Chang P, Saravanan R, Montuoro R, Nakamura H, Wu D, Lin X, Wu L (2017) Importance of resolving Kuroshio Front and eddy influence in simulating the North Pacific storm track. J Clim 30:1861–1880

Minobe S, Kuwano-Yoshida A, Komori N, Xie S-P, Small RJ (2008) Influence of the Gulf Stream on the troposphere. Nature 452:206–209

Minobe S, Miyashita M, Kuwano-Yoshida A, Tokinaga H, Xie S-P (2010) Atmospheric response to the Gulf Stream: seasonal variations. J Clim 23:3699–3719

Nakamura M, Yamane S (2009) Dominant Anomaly Patterns in the Near-Surface Baroclinicity and Accompanying Anomalies in the Atmosphere and Oceans. Part I: North Atlantic Basin. J Clim 22:880–904

Nakamura H, Sampe T, Tanimoto Y, Shimpo A (2004) Observed associations among storm tracks, jet streams and midlatitude oceanic fronts. AGU Geophys Mono Ser 147:329–345

Nakamura H, Sampe T, Goto A, Ohfuchi W, Xie S-P (2008) On the importance of midlatitude frontal zones for the mean state and dominant variability in the tropospheric circulation. Geophys Res Lett 35:L15709. https://doi.org/10.1029/2008GL034010

Neu U et al (2013) IMILAST: a community effort to intercompare extratropical cyclone detection and tracking algorithms. Bull Am Meteorol Soc 94:529–547

O'Neill LW, Haack T, Chelton DB, Skyllingstad E (2017) The Gulf Stream convergence zone in the time-mean winds. J Clim 74:2383–2412

Ogawa F, Nakamura H, Nishii K, Miyasaka T, Kuwano-Yoshida A (2012) Dependence of the climatological axial latitudes of the tropospheric westerlies and storm tracks on the latitude of an extratropical oceanic front. Geophys Res Lett 39:2011GL049922

Parfitt R, Czaja A (2016) On the contribution of synoptic transients to the mean atmospheric state in the Gulf Stream region. Q J R Meteorol Soc 142:1554–1561

Park S, Bretherton CS, Rasch PJ (2014) Integrating cloud processes in the community atmosphere model, version 5. J Clim 27:6821–6856

Piazza M, Terray L, Boe J, Maisonnave E, Sanchez-Gomez E (2016) Influence of small-scale North Atlantic sea surface temperature patterns on the marine boundary layer and free troposphere: a study using the atmospheric ARPEGE model. Clim Dyn 46:1699–1717

Putnam WM, Lin S-S (2007) Finite volume transport on various cubed sphere grids J. Comput Phys 227:55–78

Reynolds RW, Smith TM, Liu C, Chelton DB, Casey KS, Schlax MG (2007) Daily high-resolution-blended analyses for sea surface temperature. J Clim 20:5473–5496

Roberts MJ, Hewitt HT, Hyder P, Ferreira D, Josey SA, Mizielinski M, Shelly A (2016) Impact of ocean resolution on coupled air-sea fluxes and large-scale climate Geophys Res Lett 43:10430–10438. https://doi.org/10.1002/2016GL070559

Saba VS et al (2016) Enhanced warming of the Northwest Atlantic Ocean under climate change. J Geophys Res Ocean 121:118–132

Sheldon L, Czaja A, Vanniere B, Morcrette C, Sohet B, Casado M, Smith D (2017) A warm path to Gulf Stream–troposphere interactions. Tellus 69:1–13

Simpson IR, Bacmeister JT, Sandu I, Rodwell MJ (2018) Why do modelled and observed surface wind stress climatologies differ in the trade wind regions? J Clim 31:491–513

Small RJ, Tomas RA, Bryan FO (2014a) Storm track response to Ocean Fronts in a global high-resolution climate model. Clim Dyn 43:805–828

Small RJ et al (2014b) A new synoptic scale resolving global climate simulation using the community earth system model. J Adv Model Earth Syst 6:1065–1094. https://doi.org/10.1002/2014MS000363

Smirnov D, Newman M, Alexander MA, Kwon Y-O, Frankignoul C (2015) Investigating the local atmospheric response to a realistic shift in the Oyashio Sea surface temperature front. J Clim 28:1126–1147

Smith RD et al (2010), The parallel ocean program (POP) reference manual. In: Los Alamos National Laboratory technical report LAUR-10-01853

Stoelinga MT (1996) A potential vorticity-based study of the role of diabatic heating and friction in a numerically simulated baroclinic cyclone. Mon Weather Rev 124:849–874

Taguchi B, Nakamura H, Nonaka M, Xie S-P (2009) Influences of the Kuroshio/Oyashio extensions on air-sea heat exchanges and storm track activity as revealed in regional atmospheric model simulations for the 2003/04 cold season. J Clim 22:6536–6560

Trenberth KE (1991) Storm tracks in the southern hemisphere. J Atmos Sci 48:2159–2178

Vecchi GA et al (2014) On the seasonal forecasting of regional Tropical Cyclone activity. J Clim 27: 7994–8016

Ullrich PA, Zarzycki CM (2017) TempestExtremes: a framework for scale-insensitive pointwise feature tracking on unstructured grids. Geosci Model Dev 10:1069–1090

Wallace JM, Lim G-H, Blackmon ML (1988) Relationship between cyclone tracks, anticyclone tracks and baroclinic waveguides. J Atmos Sci 45:439–462

Wang CL, Zhang S-K, Lee L, Wu, Mechoso CR (2014) A global perspective on CMIP5 climate model biases. Nat Clim Change 4:201–205

Weese SR, Bryan FO (2006) Climate impacts of systematic errors in the simulation of the path of the North Atlantic current. Geophys Res Lett 33:L19708. https://doi.org/10.1029/2006GL027669

Weijer W, and co-authors (2012) The Southern Ocean and its climate in CCSM4. J Clim 25:2652–2675

Willison J, Robinson WA, Lackmann GM (2013) The importance of resolving mesoscale latent heating in the North Atlantic storm track. J Atmos Sci 70:2234–2250

Woollings T, Hoskins B, Blackburn M, Hassell D, Hodges K (2010) Storm track sensitivity to sea surface temperature resolution in a regional atmosphere model. Clim Dyn 35:341–353